

## **Adhesion Gprotein coupled receptor 56 is required for 3T3L1 adipogenesis**

Al Hasan, Mohammad; Roy, Poornima; Dolan, Sharron; Martin, Patricia E.; Patterson, Steven; Bartholomew, Chris

*Published in:*  
Journal of Cellular Physiology

*DOI:*  
[10.1002/jcp.29079](https://doi.org/10.1002/jcp.29079)

*Publication date:*  
2020

*Document Version*  
Author accepted manuscript

[Link to publication in ResearchOnline](#)

*Citation for published version (Harvard):*  
Al Hasan, M, Roy, P, Dolan, S, Martin, PE, Patterson, S & Bartholomew, C 2020, 'Adhesion Gprotein coupled receptor 56 is required for 3T3L1 adipogenesis', *Journal of Cellular Physiology*, vol. 235, no. 2, pp. 1601-1614. <https://doi.org/10.1002/jcp.29079>

### **General rights**

Copyright and moral rights for the publications made accessible in the public portal are retained by the authors and/or other copyright owners and it is a condition of accessing publications that users recognise and abide by the legal requirements associated with these rights.

### **Take down policy**

If you believe that this document breaches copyright please view our takedown policy at <https://edshare.gcu.ac.uk/id/eprint/5179> for details of how to contact us.

# **Adhesion G-Protein Coupled Receptor 56 is required for 3T3-L1 Adipogenesis**

**Authors:** Mohammad Al Hasan, Poornima Roy, Sharron Dolan, Patricia E Martin, Steven Patterson and Chris Bartholomew.

**Running title:** Gpr56 regulates adipogenesis

**Address:** Department of Biological & Biomedical Sciences, School of Health & Life Sciences, Glasgow Caledonian University, City Campus, Cowcaddens Road, Glasgow, G4 OBA, Scotland.

**Corresponding Author:** Chris Bartholomew  
email: [c.bartholomew@gcu.ac.uk](mailto:c.bartholomew@gcu.ac.uk)  
Phone: 0141-331-3213

## **Acknowledgments:**

We would like to thank the Dept. of Biological & Biomedical Sciences, GCU technical staff, Fiona Biggerstaff and Ann Marie Clark for continuous assistance throughout this project. In addition we would like to thank HONS project students Rebecca McPeak, Claire Wallace, Jonathon Willock and Rabia Ashraf for their contribution to this work. This work was supported by Glasgow Caledonian University and a PhD studentship (MAH) from the Kuwait Cultural Bureau, London, UK.

**Abstract:** Obesity-associated conditions represent major global health and financial burdens and understanding processes regulating adipogenesis could lead to novel intervention strategies. This study shows that adhesion G-protein coupled receptor 56 (*GPR56*) gene transcripts are reduced in abdominal visceral white adipose tissue derived from obese Zucker rats vs lean controls. Immunostaining in 3T3-L1 pre-adipocytes reveals both mitotic cell restricted surface and low level general expression patterns of Gpr56. *Gpr56* transcripts are differentially expressed in 3T3-L1 cells during adipogenesis. Transient knockdown (KD) of *Gpr56* in 3T3-L1 cells dramatically inhibits differentiation through reducing the accumulation of both neutral cellular lipids (56%) and production of established adipogenesis Ppar $\gamma_2$  (60-80%), C/ebp $\alpha$  (40–78%) mediator and Ap2 (56-80%) marker proteins. Furthermore, genome editing of *Gpr56* in 3T3-L1 cells created CW2.2.4 and RM4.2.5.5 clones (*Gpr56*<sup>-/-</sup> cells) with compound heterozygous deletion frameshift mutations which abolish adipogenesis. Genome edited cells have sustained levels of the adipogenesis inhibitor  $\beta$ -catenin, reduced proliferation, reduced adhesion, altered profiles and or abundance of extracellular matrix component gene transcripts for fibronectin, types I, III and IV Collagens and loss of actin stress fibres.  $\beta$ -catenin KD alone is insufficient to restore adipogenesis in *Gpr56*<sup>-/-</sup> cells. Together these data show that Gpr56 is required for adipogenesis in 3T3-L1 cells. This report is the first demonstration that Gpr56 participates in regulation of the adipogenesis developmental programme. Modulation of the levels of this protein and/or its biological activity may represent a novel target for development of therapeutic agents for the treatment of obesity.

**Key Words:** *GPR56*; Adipogenesis; Knockdown; Genome editing;  $\beta$ -CATENIN; Extracellular matrix.

**Introduction:** Obesity and associated diseases including type II diabetes, heart disease and cancer represent major global health and financial burdens and understanding the molecular basis of adipogenesis could identify novel therapeutic strategies for treatment. G-protein coupled receptors (GPCR's) are involved in the regulation of adipose tissue but in many cases their function has not been investigated. GPCR's comprise a large gene family of which adhesion G-protein coupled receptors represent a sub-group of 33 members in the human genome (Mehta & Piao, 2017). *GPR56* (*ADGRG1*) is a member of this sub-group and the encoded protein is associated with brain cortical patterning. Well characterised mutations of *GPR56* cause a rare autosomal recessive brain deformity, associated with severe mental retardation, motor and language impairment and epilepsy, called bilateral frontoparietal microgyria (Piao et al., 2004). *Gpr56* null mice display a defect in adhesion of developing neurons (Koirala et al., 2009) and despite the apparent absence of further phenotypic defects in these animals, *GPR56* has also been associated with other biological roles including pancreatic  $\beta$ -cell function (Duner et al., 2016), muscle hypertrophy (White et al., 2014), tumorigenesis (Aust et al., 2016) and maintenance of haemopoietic stem cells (Rao et al., 2015)(Saito et al., 2013).

*GPR56* is expressed in adipocytes (Amisten et al., 2015) and several observations are consistent with a possible role in adipogenesis. Two ligands have been identified for *GPR56*, type III collagen [*COL3A1*] (Luo et al., 2011) and transglutaminase 2 [*TGM2*] (Xu et al., 2006). *TGM2* is present in white adipose tissue and has been shown to inhibit adipogenesis in *Tgm2* null mouse embryo fibroblasts (Myneni et al., 2015). The absence of *Tgm2* correlates with reduced nuclear  $\beta$ -catenin, a negative regulator of adipogenesis (Ross et al., 2000), as well as reduced Rock kinase activity. *COL3A1* stimulates RHOA when bound to *GPR56* in neural progenitor cells via activation of the  $\alpha$  subunits of heterotrimeric  $G_{12/13}$  proteins (Iguchi et al., 2008). A role for a cryptic GPCR in adipogenesis is suggested by *Pasteurella multocida* toxin mediated activation of  $G_{12/13}$  protein subunits resulting in suppression of 3T3-L1 cell differentiation (Bannai et al., 2012). Activation of  $G_{12/13}$  protein subunits stimulate RHOA which in turn activates ROCK1 and ROCK2 kinases. Pharmacological inhibition of Rock2 kinase with Y27632 in 3T3-L1 cells mediates differentiation to adipocytes in the absence of the normal chemical cocktail required to execute this development programme (Papers & Doi, 2007). Thus, evidence suggests that stimulation of the  $G_{12/13}$   $\alpha$  protein/RHOA/ROCK pathway inhibits adipogenesis. Therefore, modulation of adipogenesis

93 by the same proteins which mediate GPR56 signalling indicates a potential link with this  
94 developmental programme.

95 The fibroblast-like 3T3-L1 cell line is a valuable model system to study adipogenesis (Todaro  
96 & Green, 1963). Hormonal stimulation initiates differentiation into an adipocyte-like  
97 phenotype and induction of a cascade of transcription factors mediating adipogenesis  
98 including key regulator CAAT enhancer binding proteins (C/EBP) (Cao et al., 1991) and  
99 peroxisome proliferator activated receptor proteins (PPAR) (Tontonoz et al., 1994).  
100 C/EBP $\beta$  is rapidly and transiently induced and regulates the production of C/EBP $\alpha$  and  
101 PPAR $\gamma$  which in turn control expression of target genes required for adipogenesis. Enforced  
102 expression or depletion of C/EBP $\beta$ , inhibits and enhances adipogenesis respectively  
103 (Schroeder-Gloeckler et al., 2007). PPAR $\gamma$  is essential to execute this developmental  
104 programme (Rosen et al., 2002).

105 The current study characterises the expression of *GPR56* in adipose tissue from lean and  
106 obese rats and 3T3-L1 cells and investigates the role of GPR56 in adipogenesis by  
107 knockdown and genome editing in these cells.

108

109

110

## Materials and Methods

**Animal studies** All studies were approved by the Institute's Animal Welfare and Ethical Review body and carried out in accordance with the UK Animals Scientific Procedures Act (1986).

**Zucker Rats** Abdominal visceral white adipose tissue was collected from obese Zucker male rats (*fa/fa*; n=6) and lean male littermates (*fa/-*; n=6), purchased from Harlan laboratories (UK). Animals were aged 17-20 wks with mean weights of 374.2g, SEM 51.8g (Lean) and 559.5g, SEM 27.6g (Obese). Animals were euthanized by intraperitoneal administration of pentobarbital (5mg/100g) [pharmasol, JM Loveridge PLC, Southampton, UK] and tissues collected and immediately stored at -80C.

**Preparation of Total Cellular RNA, cDNA Synthesis and Quantitative Real-time Polymerase Chain Reaction** RNA was prepared from cultures of cells by the TRI Reagent® method (Sigma-Aldrich, 93289). RNA from adipose tissue was prepared by first homogenizing 50mg of sample in 1ml TRI Reagent with 50µl 0.1mm glass beads (Biospec products Inc, Bartlesville, Oklahoma, U.S.A.) using a FASTPREP FP120 (Thermo Electron Corporation, Beverly, Massachusetts, U.S.A.). One µg of total cellular RNA was used to synthesise cDNA using SuperScript III First-Strand Synthesis SuperMix cDNA synthesis kit (Invitrogen, 18080) according to the manufacturer's instructions. 1.5 % of the cDNA reaction was used for quantitative real-time polymerase chain reaction using SYBR Green Rox mix (Thermo Fisher Scientific, Waltham, Massachusetts, U.S.A., 11873913), gene specific oligonucleotide primers, 95°C, 15mins followed by 40 cycles 95°C, 15s, 60°C, 60s in a CFX96 C1000 Thermal cycler (BIO-RAD Laboratories Ltd., Hemel Hempstead, UK). Relative expression levels between target and calibrator genes were determined using the arithmetic comparative  $2^{-\Delta\Delta C_t}$  method (Livak & Schmittgen, 2001).

**Cell Culture** 3T3-L1 (ATCC®CL-173™) cells were cultured in complete medium (CM) comprising Dulbecco's Modified Eagle's Medium (Lonza Group Ltd, Basel, Switzerland, BE12-604F) supplemented with 10% v/v newborn calf serum (3T3-L1) (Sigma-Aldrich, Poole, UK, N4637) and 2.5mM glutamine, 50units/ml penicillin, 50µg/ml streptomycin (Lonza Group Ltd, BE17-605E & BE17-603E), 37°C, 5% CO<sub>2</sub>. For differentiation, 3T3-L1 were maintained at 100% confluence for 48hrs prior to supplementing with induction medium 1 (IM1), comprising CM with 10% v/v foetal calf serum (Lonza, DE14-801F), 5µg/ml insulin (Sigma-Aldrich, I9278), 0.25µM dexamethasone (Sigma-Aldrich, D4902), 0.5mM Isobutylmethylxanthine (IBMX, Sigma-Aldrich I5879) for 48hrs, followed by

incubation with induction medium 2 (IM2) comprising CM supplemented with 10% FCS and 5µg/ml insulin every 48hrs up to 10 days. siRNA transfected cells were induced to differentiate as above 72hrs post-transfection. For genome editing, semi-confluent cultures of 3T3-L1 cells were transfected with 1µg each recombinant gRNA, hCas9 (gift from George Church, Addgene plasmid # 41824 and 41815 (Mali et al., 2013)) and pC1 (recombinant pSIREN-RetroQ vector [Clontech, Mountain View, California, USA, 631526] with scrambled control shRNA inserted (*Bartholomew, unpublished*)) plasmid DNA's using Lipofectamine 3000 (ThermoFisher Scientific Inc., St. Leon-Rot, Germany, L300000) according to manufacturer, 48hrs, then CM supplemented with 2µg/ml puromycin (Sigma-Aldrich, P8833) 96hrs. Single cell clones were derived from isolated colonies. Media was removed from cells which were then rinsed with Phosphate buffered saline (PBS, Lonza, BE17-516F), overlaid with trypsin-EDTA (Lonza BE17-161E) saturated sterile filter paper discs (Whatmann 1MM, Fisher Scientific, Loughborough, UK), incubated for 5mins, 37°C and discs plus cells transferred to 24 well culture dish with 500µl CM. Cell numbers were determined using a haemocytometer counting chamber (Neubauer Marienfeld, Paul Marienfeld GmbH & Co. KG, Germany) and inverted microscope (CK2, Olympus UK Ltd, Southend-on Sea, UK).

**Immunostaining** Cells were cultured on sterile 16mm<sup>2</sup> microscope coverslips, washed with ice cold PBS and fixed with ice cold 4% w/v paraformaldehyde for 10mins at room temperature (rt). Permeabilised cells were treated with 0.1% (v/v) Triton™ X-100 (Sigma-Aldrich, T8787) in PBS, 10 min, rt then washed in PBS 15min, rt. Both permeabilised and non-permeabilised cells were incubated 60mins, rt in blocking buffer (PBS, 0.2M glycine, 10% v/v FCS) then o/n, 4°C, with primary antibody α-GPR56 (Merck KGaA, Darmstadt, Germany, H11) or α-VSVG (Santa Cruz Biotechnology Inc, Santa Cruz, CA, U.S.A., F-6). Cells were washed 40mins at rt in PBS and incubated for 1.5hr at rt with secondary antibody Goat α-mouse IgG H&L Alexa Fluor® 488, (abcam ab150113) in blocking buffer. Cells were washed in PBS for 1hr at rt, counterstained with DAPI-hydrochloride (ThermoFisher, D1306) for 1min at rt and washed in PBS for 1min at rt and then mounted with Fluorosave™ (Millipore 345789). Alternatively, fixed, permeabilised cells were incubated with 165nM Alexa Fluor™ 488 Phalloidin (A12379, Invitrogen) in PBS, 1hr at rt and washed and stained with DAPI as above. Image acquisition was performed using a LSM 800 confocal microscope with a 63Å~1.4 NA oil immersion objective using ZEN 2.3 (blue edition) software (Carl Zeiss GmbH, Jena, Germany).

**Oil Red O Staining and Quantitation**

Cells were washed in ice cold PBS, fixed in 10% v/v formaldehyde for 10 minutes at room temperature (rt) and incubated sequentially in 60% isopropanol for 1 hour at rt in 6% w/v Oil Red O (Sigma-Aldrich, O0625, in 60% isopropanol), then ice cold PBS. For quantitation, Oil Red O stain was extracted with 50% culture volume of 100% isopropanol for 5 minutes and absorbance read at 492nm using an Epoch plate reader (Biotek Instruments Inc, Plainfield, NJ, USA).

**Oligonucleotide Primers**

Oligonucleotide primers were synthesised by Integrated DNA Technologies (IDT, BVBA, Leuven, Belgium) (see table below for sequences).

Gpr56F: CCGAGCTTCATCTTCTCCTTC	Gpr56R: GCTGCTGCAATTCCTTCTTG
18SF: ACCGCAGCTAGGAATAATGGA	18SR: GCTTCAGTTCCGAAAACCA
ratgpr56F: CTAACCTCTCAGATCCCGTGGTA	ratgpr56R: CACACTGCAGAGTCACGTTCTTT
gapdhF: CTGACATGCCGCCTGGAGAAA	gapdhR: CCACCCTGTTGCTG TAGCCAT
Ppar $\gamma$ 2F: GCCCACCATTCCGGCAATC	Ppar $\gamma$ 2R: TGCGAGTGGTCTTCCATCAC
C/ebp $\alpha$ F: GAGCTGAGTGAGGCTCTCATT	C/ebp $\alpha$ P: TGGGAGGCAGACGAAAAAAC
Ap2F: GGGCATGGAATTTCGATGAAATCA	Ap2R: CCCGCCATCTAGGGTTATGAT
$\beta$ -cateninF: ACTAAGCAGGAAGGGATGGA	$\beta$ -cateninR: ATGACGAAGAGCACAGATGG
JWgF: TTTCTTGGCTTTATATATCTTGTGGAAA GGACGAAACACCGGATAGAGCCCTCTAGGCTC	JWgR: GACTAGCCTTATTTAACTTGCTATTT CTAGCTCTAAAACGAGCCTAGAGGGGCTCTA TC
RMgF: TTTCTTGGCTTTATATATCTTGTGGAAA GGACGAAACACCGGGAGACTCCACTTGCGCTA	RMgR: GACTAGCCTTATTTAACTTGCTATTT CTAGCTCTAAAACGAGCAAGTGGAGTCTC C
Alt-RF: GAGAAGACTTCCGCTTCTGTG	Alt-RR CTCCATCCCTTGTCTCTGTG
RAF: GCTCTATCACTTCTGCCTCTAC	RAR: AATCTGCCAGGAGCTGAC
JWF: CAGAGGAGACCCTCACAATTC	JWR: CTTGGCTACTAAGCAGGTAGTC
Fn1F: TACGGAGAGACAGGAGGAAATA	Fn1R: CATAAGGGTGATGGTGTAGTC
Col1 $\alpha$ 1F: AGACCTGTGTGTTCCCTACT	Col1 $\alpha$ 1R: GAATCCATCGGTCATGCTCTC
Col3 $\alpha$ 1F: CTGTAACATGGAACTGGGGAAA	Col3 $\alpha$ 1R: CCATAGCTGAACTGAAAACCA CC
Col4 $\alpha$ 1F: GGTCTGTCTGGAAGAGTTTAG	Col4 $\alpha$ 14R: TGAACATCTCGTTCTCTCTATG
Col6 $\alpha$ 1F: TGCCCTGTGGATCTATTCTTCG	Col6 $\alpha$ 1R: CTGTCTCTCAGGTTGTCAATG
LKO.1: GACTATCATATGCTTACCGT	

**siRNA-Mediated Gene Knockdown**

2X10<sup>4</sup> 3T3-L1 cells were seeded in a 24-well plate, cultured for 24hrs then transfected with *Gpr56* 30nM Dicer-Substrate siRNAs, G-DsiRNA 1, 2, 3 or S. DsiRNA (IDT, #157187617, #157187609, #157187606, #51-01-19-09) or  $\beta$ -catenin Dicer-Substrate siRNAs BcatsiRNA's 1, 2 and 3 (IDT, #76963822, #7696819, #76963816), using Lipofectamine<sup>TM</sup> RNAiMAX for 48hrs according to the manufacturer's instructions (Invitrogen, 13778030).

**Western Blot Analysis**

Cultured cells were mechanically harvested in ice-cold RIPA buffer (1% NP-40, 50mM TrisPH7.6, 120mM NaCl, 1mM EDTA) containing protease inhibitor cocktail (P8340) and phosphatase inhibitor cocktail 3 (P0044) (Sigma-Aldrich), incubated on ice for 30mins then centrifuged 13,000rpm, 20mins at 4°C. Protein concentration was



determined using the Bicinchoninic acid protein assay method (Stoscheck, 1990). Equal quantities of proteins were separated by SDS-polyacrylamide gel electrophoresis and transferred to nitrocellulose. Nitrocellulose bound total protein was used for quantification using the REVERT™ total protein stain kit according to the manufacturer's instructions (926-1101, LI-COR™, Lincoln, Nebraska, U.S.A.) and analysed at 700nm using an Odyssey FC image analyser (LI-COR®). Subsequently, membranes were washed in REVERT™ reversal solution and western blotting performed with antibodies to  $\alpha$ -GPR56 (Merck, H11),  $\alpha$ -PPAR $\gamma$  (C26H12),  $\alpha$ -C/EBP- $\alpha$  (2295),  $\alpha$ - $\beta$ ACTIN (8H10D10), Total  $\beta$ -catenin (D10A8), Active  $\beta$ -catenin (D13A1) (Cell Signaling Technologies®, Leiden, The Netherlands), or  $\alpha$ -AP-2 (Santa Cruz Biotechnology Inc, C-15) at 1:1000 dilution. Appropriate IRDye®800CW conjugated  $\alpha$ -goat (926-32214), IRDye®800CW conjugated  $\alpha$ -rabbit (926-32211) or IRDye®680RD conjugated  $\alpha$ -mouse (926-68072) (LI-COR®) IgG secondary antibodies were used at 1/15000 dilutions. Detection was performed by fluorescence using an Odyssey FC image analyser (LI-COR®) and analysed with Image Studio Software Lite Ver 5.2 (LI-COR®).

#### ***Creation of Retroviral and gRNA Vectors and Preparation of Plasmid DNA***

Guide RNA (gRNA) plasmid vectors pCW2 and pRM4 were created using the gRNA cloning vector (gift from George Church Addgene ID 41824) (Mali et al., 2013). CRISPR targets in murine *Gpr56* exon 3 sequence (Adgrg1-202, ENSMUST00000179619.8) were identified using a CRISPR design tool (<http://crispr.mit.edu>). Two target sequences were selected and oligonucleotides CWgF, CWgR RMgF and RMgR synthesized. Primer annealing and extension was performed with 0.5 $\mu$ M each of either CWF and CWR or RMF and RMR in 1X 5XPhusion® HF buffer, 200 $\mu$ M dNTP's, 1 unit Phusion® DNA polymerase (New England Biolabs, M0530) in 50 $\mu$ l, 98°C 30sec, 40 cycles of 98°C 10sec, 52°C 30sec, 72°C 30sec followed by 72°C 2mins in a MJ Scientific programmable thermocycler. Annealed DNA was gel-purified (Nucleospin® Gel and PCR clean-up). *Bsp*TI (ThermoFisher Inc., ER0831) linearised gRNA cloning vector and annealed DNA fragments were combined with Gibson assembly master mix (New England Biolabs, E5510) in 10 $\mu$ l and incubated 50°C, 1h and 2 $\mu$ l used to transform NEB 5-alpha high efficiency competent cells (New England Biolabs, E5510). All plasmid DNA was prepared by affinity chromatography using Nucleobond® PC500EF gravity flow columns according to manufacturer's instruction (Macherey-Nagel GmbH). pCW2 and pRM4 gRNA target sequence was confirmed using LKO.1 primers.

***Isolation of Genomic DNA and Heteroduplex Analysis*** DNA was isolated from 10,000-15,000 cells in 96 well culture dish using 50 $\mu$ l QuickExtract DNA isolation solution

229 (Lucigen, Cambridge, UK, QE09050), vortexed 30sec, incubated 65°C 10 mins, 98°C 5 mins  
230 and diluted in 100µl nuclease free water. DNA was amplified with 40ng genomic DNA,  
231 300nM Alt-RF and Alt-RR primers, 1X DreamTaq Green PCR master mix  
232 (ThermoScientific, K1081) in 25µl, 95°C 90sec, 40 cycles 95°C 30sec, 65°C 30secs, 72°C 30  
233 sec and 72°C 5mins using a MJ Scientific programmable thermocycler. Amplified DNA  
234 (20%), 1X T7EI reaction buffer (Alt-R Genome Editing Detection Kit, Integrated DNA  
235 Technologies, 1075932) in 10µl was denatured 95°C 10mins, annealed 95-85°C (Ramp rate -  
236 2°C/sec), 85-25°C (Ramp rate -0.3°C/sec) and digested 1U T7 DNA endonuclease 1 hour  
237 37°C in a MJ Scientific programmable thermocycler.

238 **Identification of Mutant Alleles** Genomic DNA was amplified by PCR with either  
239 RAF/RAR (RM cells) or JWF/JWR (CW cells) primers with DreamTaq as described above.  
240 Amplified DNA was inserted into pJET1.2 cloning vector using CloneJET PCR cloning kit  
241 (ThermoScientific, K1231) according to manufacturer's instructions and used to transform  
242 DH5-α competent cells (Invitrogen, 18265-017). Individual colonies were picked for colony  
243 PCR with pJET1.2 Forward and Reverse primers (ThermoScientific, K1231) with DreamTaq.  
244 Amplified DNA was sequenced using the pJET1.2 Forward primer.

245 **Sequencing** Sequences were determined by Sanger sequencing of plasmid and PCR  
246 amplified DNA using the automated LIGHTRUN™ DNA sequencing service (Eurofins  
247 Genomics, Constance, DE). DNA sequence analysis was performed using SnapGene DNA  
248 viewer 3.3.4.

249 **Cell Proliferation assay** The AlamarBlue® cell proliferation assay (DAL1025,  
250 Invitrogen™) was used according to manufacturer's instructions.  $5 \times 10^2$  cells/well were  
251 seeded in 96 well plates in CM and refed every 24hrs. Metabolic activity was determined  
252 every 24hr in CM supplemented with 10% AlamarBlue® for 4hr. AlamarBlue® reduction was  
253 determined from absorbance at 570nm and 600nm using a FLUOstar® Omega plate reader  
254 (BMG LABTECH LTD).

255 **Cell Adhesion Assay** One thousand cells/well were seeded in CM and incubated in 96 well  
256 plates for 6hr, 37°C, 5% CO<sub>2</sub>. Medium was removed, cells washed in PBS, fixed with 10%  
257 (v/v) formaldehyde in PBS 10min rt, rinsed 2X with PBS then stained with 0.1% (w/v)  
258 crystal violet (CO775, Sigma- Aldrich) in 2% ethanol 10 min, rt. Cells were washed in PBS,  
259 crystal violet extracted in 2% SDS then absorbance 570nm determined with an Epoch plate  
260 reader.

261 ***Statistical Analysis*** Data are expressed as the mean  $\pm$  standard error of the mean from at  
262 least 3 independent experiments. Statistical significance was determined by one-way  
263 ANOVA, two-way ANOVA, unpaired two-tailed Student t-test or multiple t-test as indicated,  
264 using GraphPad PRISM<sup>®</sup> 7.0c software.  $P \leq 0.05$  was considered significant.  
265

## Results

### GPR56 is Differentially Expressed in Adipose Tissue and 3T3-L1 cells

The abundance of *GPR56* gene transcripts was compared in abdominal visceral white adipose tissue from lean vs obese Zucker rats by reverse-transcription quantitative real-time polymerase chain reaction (QPCR) with oligonucleotide primers specific for rat *gpr56* (ratgpr56F&R) as described in Materials and Methods. Levels of *gpr56* gene transcripts were significantly lower in white adipose tissue from obese (50-60% reduction) vs lean rats (Fig.1A).

We next examined *Gpr56* expression in 3T3-L1 preadipocytes. Immunostaining with  $\alpha$ -*Gpr56* showed a low level of either general staining (Fig.1B, + permeabilised) in all cells or punctate cell surface staining that is observed in mitotic cells only (Fig.1B, - non-permeabilised). Next *Gpr56* gene expression was investigated at various stages of the adipogenesis differentiation programme. Cultures of 3T3-L1 cells were induced to differentiate and at various time points either stained with Oil Red O or total cellular RNA isolated for QPCR (Materials and Methods). An increased accumulation of Oil-red O stained neutral lipids (Fig.1C) and gene transcripts of regulators and markers (*C/ebp $\alpha$* , *Ppar $\gamma$* <sub>2</sub>, adipocyte factor 2 *Ap2*, data not shown) was observed in 3T3-L1 cells as differentiation progressed confirming execution of the adipocyte developmental program. QPCR results confirmed *Gpr56* gene transcripts in 3T3-L1 cells (Fig.1D). Expression levels vary moderately with an initial decline followed by an increase reaching maximum levels 6 day's post-induction (Fig.1D).

### *Gpr56* Knockdown Inhibits 3T3-L1 Cell Adipocyte Differentiation

The impact of loss of endogenous *Gpr56* on 3T3-L1 differentiation was investigated by gene knockdown (KD) using Dicer-Substrate Short Interfering RNAs (DsiRNA's). *Gpr56* KD efficiency of three DsiRNAs, targeting exons 3, 11 or 14 (Fig.2A) were tested. All three KD 3T3-L1 *Gpr56* gene transcripts (S1A) and the most effective, G-DsiRNA 2 (90% KD), was selected for further analysis.

Initially KD of *Gpr56* transcripts was examined in 3T3-L1 cells through differentiation for up to 10 days. *Gpr56* transcripts initially decline between 0 and 2 days with control S- siRNA (scrambled) and then are induced in days 3, 4, 6 and 10 (Fig.2B) in a similar manner to untreated 3T3-L1 cells (Fig.1D). However, G-DsiRNA 2 treated 3T3-L1 cells show decreased *Gpr56* transcripts in both pre-adipocytes and through the differentiation program

although again expression increases from day 3 to 10 (Fig.2B, S siRNA vs G-DsiRNA 2). Cells are transfected once with DsiRNA's (Materials and Methods) and therefore the late increase in transcripts show inhibition of *Gpr56* expression is only transient. 3T3-L1 cells were also immunostained with  $\alpha$ -Gpr56 24hrs post-transfection with either control S- siRNA or G-DsiRNA 2 (Fig.2C). The results show a significant reduction of general staining in G-DsiRNA 2 vs S-siRNA treated cells (66%, S1B), confirming a reduction in Gpr56 protein in KD cells.

G-DsiRNA 2 treatment dramatically inhibits 3T3-L1 cell adipogenesis, significantly reducing the accumulation of neutral lipid staining with Oil-red O at both days 4 and 10 by 64% and 56% respectively (Fig.3A, S1C). In contrast control, scrambled DsiRNA had no effect on 3T3-L1 cell neutral lipid accumulation (Fig.3A, S1C). Inhibition of 3T3-L1 cell differentiation was also observed with the alternative G-DsiRNA 1 (S2). Western blot analysis showed Ppar $\gamma_2$ , C/ebp $\alpha$  and Ap2 proteins are induced during differentiation of both scrambled S. siRNA and DsiRNA 2 transfected 3T3-L1 cells (Fig.3B) but quantitative analysis reveals a significantly reduced accumulation in DsiRNA 2 treated cells at days 4 (Ppar $\gamma_2$ -80%, C/ebp $\alpha$ -78%, Ap2-80%) and 10 (Ppar $\gamma_2$ -60%, C/ebp $\alpha$ -40%, Ap2-56%) (Fig.3B, S1C). QPCR analysis also shows a significant reduction in *Ppar $\gamma_2$*  (35%-50%) and *Ap2* (23%-70%) gene transcripts at days 4, 6 and 10 in G-DsiRNA 2 vs control S. siRNA treated cells (S3), consistent with western blot analysis. Sustained active  $\beta$ -catenin inhibits adipogenesis (Ross et al., 2000) and this was also investigated by Western blot analysis. Results show a reduction in active  $\beta$ -catenin at day 4 (48%) and 10 (72%) relative to day 0 in control S. siRNA differentiating 3T3-L1 cells whereas levels are initially higher (168%, day 0 G-DsiRNA 2 vs S. siRNA treated 3T3-L1 cells) and decline only moderately throughout differentiation of DsiRNA 2 treated cells (Fig. 3B, S1D).

*Inhibition of Adipogenesis in Gpr56 Genome Edited 3T3-L1 cells* To investigate the role of Gpr56 further, genome edited 3T3-L1 cell lines were created with targeted *Gpr56* gene mutations. Two sites within the *Gpr56* gene were selected for genome editing and guide RNA (gRNA) plasmid vectors pCW2 and pRM4, which target sequences within exon 3 as shown in Fig.2A, were created (Materials & Methods). 3T3-L1 cells were transfected with gRNA, pCAS9 and pC1 plasmid DNA's, transiently selected with puromycin and single cell cloned as described in Materials and Methods. Single cell clones were screened for the presence of INDELS in the *Gpr56* gene by heteroduplex analysis (S4 A). A DNA cloning and sequencing

strategy was adopted to screen cell clones for INDEL frameshift mutations (Materials and Methods). A total of 17 pCW2 (CW cells) and 21 pRM4 (RM cells) derived single cell clones with INDELS were sequenced and 3 clones with compound heterozygous deletion frameshift mutant *Gpr56* alleles identified. The partial sequences of the mutant alleles in clones CW2.2.4 and RM4.2.5.5, which were chosen for further study, are shown in Figure 4. Immunostaining with  $\alpha$ -Gpr56 in CW2.2.4 and RM4.2.5.5 cells revealed both significantly reduced staining (75%-84 %) as well as a change in cellular localisation compared to parental 3T3-L1 cells (S4 B, C), confirming loss of expression.

Adipogenesis in genome edited cells was determined by Oil Red O staining (Materials and Methods). CW2.2.4, RM4.2.5.5 and 3T3-L1 cells were induced to differentiate (Materials and Methods) and cells stained at days 0, 4 and 10. The results show the expected accumulation of Oil Red O stained neutral cellular lipids in 3T3-L1 cells at days 4 and 10 but a dramatic and highly significant reduction in staining of both genome edited cell lines (76-77% day 4 and 87-88% day 10) (Fig.5A, S5 A). Furthermore, Western blot analysis showed no significant induction of Ppar $\gamma$ <sub>2</sub>, C/ebp $\alpha$  and Ap2 proteins in RM4.2.5.5 cells (Fig.5B, S5 B), which is consistent with Oil red O staining data. Western blotting again showed sustained active  $\beta$ -catenin in differentiating genome edited cells (Fig.5B, S5 B).  $\beta$ -catenin KD was used to see if adipogenesis could be restored in RM4.2.5.5. BcatisRNA 3 was chosen from three DsiRNA's tested as it significantly reduced total  $\beta$ -catenin protein (92%) in 3T3-L1 cells (S6 A, B, C) but treatment of RM4.2.5.5 cells failed to restore adipogenesis (S6 D).

#### *Gpr56 genome edited cells show reduced proliferation, adhesion, actin stress fibres and altered extracellular matrix gene expression*

*Gpr56* is associated with cell proliferation and adhesion and these properties were examined to further investigate the impact of *Gpr56* loss in 3T3-L1 cells. Results show that both RM4.2.5.5 and CW2.2.4 cell lines have significantly reduced proliferation rates vs 3T3-L1 cells (Fig.6A). Furthermore, both cell lines show significantly reduced adhesion compared with parental cells (Fig.6B). Gene transcripts encoding extracellular matrix (ECM) proteins fibronectin (*Fn1*) and types I (*Col1 $\alpha$ 1*), III (*Col3 $\alpha$ 1*) IV (*Col4 $\alpha$ 1*), VI (*Col6 $\alpha$ 1*) collagens were compared by QPCR (Materials and Methods) in preadipocytes (day 0) and at 10 days post differentiation in 3T3-L1 vs RM4.2.5.5 cells. The results show significant differences for *Fn1*, *Col1 $\alpha$ 1* and *Col4 $\alpha$ 1* gene transcripts in the presence (3T3-L1) and absence of *Gpr56* (RM4.2.5.5). Normally, *Fn1* and *Col1 $\alpha$ 1* gene transcripts decline and *Col4 $\alpha$ 1* and *Col6 $\alpha$ 1* transcripts increase as 3T3-L1 cells

differentiate (Fig.6C). However, *Fn1* is significantly decreased in preadipocytes (74% reduction in RM4.2.5.5 vs 3T3-L1) and induced 4 fold at 10 days in RM4.2.5.5 relative to 3T3-L1. *Col1 $\alpha$ 1* transcripts are significantly elevated in preadipocyte RM4.2.5.5 cells (>2 fold in 3T3-L1 vs RM4.2.5.5) and decline to 3T3-L1 cell levels at day 10. *Col4 $\alpha$ 1* transcripts are similar in both preadipocyte cells but significantly less at 10 days differentiation in RM4.2.5.5 vs 3T3-L1 (reduced 74%). The level of *Col3 $\alpha$ 1* are slightly increased in RM4.2.5.5 relative to 3T3-L1 cells but decline in both cases during differentiation. The levels and induction of *Col6 $\alpha$ 1* during differentiation are the same in both cell types (Fig.6C). Significant changes in the organization of the actin cytoskeleton occur during differentiation of adipocytes (Nobusue et al., 2014). To examine actin cytoskeleton, 3T3-L1 and RM4.2.5.5 preadipocytes were stained with fluorescently labelled Phalloidin (Materials and Methods). The results show a significant difference in F-actin organization (Fig.7A) and quantity (Fig.7B) in RM4.2.5.5 vs 3T3-L1 cells. 3T3-L1 cells show F-actin organized in stress fibres whereas RM4.2.5.5 cells show reduced, thin stress fibres, staining of the cell cortex (Fig.7A) and generally reduced staining intensity (Fig.7B, 25% reduction).

## Discussion

Several GPCR's regulate adipogenesis (Eisenstein, 2013) and GPR56 expression has been observed in adipocytes previously (Amisten et al., 2015). In this study, we show for the first time that GPR56 is necessary for adipogenesis *in vitro*. Data generated from our *in vitro* studies show both KD and genome editing of GPR56 is inhibitory. The finding that levels of *gpr56* transcripts are lower in adipose tissue from genetically obese rats supports the hypothesis that dysregulation of expression of this receptor may be linked to adipocyte hypertrophy or hyperplasia. The impact of complete loss of Gpr56 on adipogenesis *in vivo* is unknown but knockout mice fed a high fat diet have a metabolic phenotype, but similar weight gain, compared to wild type animals (Spaethling et al., 2016). Further studies are required to investigate the expression of *Gpr56* in fat depots in these and other genetic and diet induced animal models of obesity to extend the observations made here.

Our results show that low levels of endogenous Gpr56 protein are seen in 3T3-L1 preadipocytes. Confocal analysis shows a general staining of cells, not seen with either isotype control or secondary antibody control antibodies, in permeabilised cells. The reduction in staining observed with both Gpr56 KD and genome edited cells confirms this is Gpr56. It is not clear why residual staining is still observed in the Gpr56 genome edited (*Gpr56*<sup>-/-</sup>) cells, but it could be due to production of a truncated protein that retains the epitope recognized by the antibody used for this study.

Low levels of cell surface Gpr56 are also detected in immunostained non-permeabilised 3T3-L1 preadipocytes. Interestingly, we only detect cell surface staining in mitotic cells, suggesting its localization might be regulated during cell division and/or contribute to this process. The significance of this M-phase specific staining requires further investigation but is consistent with other studies that suggest GPR56 participates in cell proliferation (Ackerman et al., 2015)(Bae et al., 2014).

Both KD and *Gpr56*<sup>-/-</sup> cells show that loss of Gpr56 reduces or abolishes adipogenesis in 3T3-L1 cells as demonstrated by reduced accumulation of: 1) neutral cellular lipids; 2) developmental marker protein Ap2 and 3) key regulators of adipocyte differentiation, Ppar $\gamma$ <sub>2</sub> and C/ebp $\alpha$ . The *Gpr56*<sup>-/-</sup> cell phenotype is more severe than the KD phenotype. KD results in only a transient reduction in *Gpr56* in preadipocytes at the early stages of differentiation, as transcripts recover at later stages of the developmental programme (Fig.2B days 6 and 10). This suggests Gpr56 is important at early stages of the process. The partial differentiation observed in KD cells could be due to either insufficient reduction of Gpr56 or an overall delay to the process which can still occur as levels recover. Alternatively Gpr56



might be required for both early and late events in adipogenesis which could also explain the complete abrogation of differentiation observed in *Gpr56*<sup>-/-</sup> cells. This possibility is consistent with the biphasic expression pattern observed for *Gpr56* transcripts from preadipocytes through to adipocytes. In the current study 3T3-L1 cells were found to express low levels of endogenous *Gpr56* gene transcripts which consistently vary during differentiation with an initial decrease followed by a subsequent increase that plateaus at 6 to 10 days (Fig.1D, Fig.2B). It is unclear if the biphasic change in *Gpr56* transcripts is required for differentiation as it is unknown if this coincides with changes in protein production.

The data presented suggest *Gpr56* modulates adipogenesis through changes in the production of known regulators of this process. PPAR $\gamma$  is a master regulator of adipogenesis and can initiate the entire differentiation program (Farmer, 2006) even in the absence of another key regulator of this developmental pathway, C/EBP $\alpha$  (Rosen et al., 2002). Levels of Ppar $\gamma_2$  and C/ebp $\alpha$  are both reduced with decrease or loss of *Gpr56* and therefore are most likely to be responsible for the inhibition of differentiation observed. The decreases in Ppar $\gamma_2$  and C/ebp $\alpha$  are greater in *Gpr56*<sup>-/-</sup> cells vs KD cells which correlates with severity of suppression of adipogenesis.

A potential model for the impact of *Gpr56* loss on adipogenesis is shown in figure 8. The mechanism of inhibition is unknown but could involve changes to one or more of:- 1)  $\beta$ -catenin; 2) cell proliferation; 3) cell adhesion; 4) ECM and 5) actin cytoskeleton. Numerous studies show that changes to any of these properties affect adipogenesis. Active  $\beta$ -catenin is a known inhibitor of adipogenesis and Ppar $\gamma_2$  gene expression (Okamura et al., 2009) and studies suggest a link between *Gpr56* and  $\beta$ -catenin activity (Shashidhar et al., 2005). However,  $\beta$ -catenin KD alone is insufficient to restore adipogenesis in *Gpr56*<sup>-/-</sup> cells suggesting other inhibitory mechanisms also contribute. Stimulation of cell proliferation inhibits adipogenesis (Hu et al., 1996) (Heath et al., 2000) (Abbott & Holt, 1997). GPR56 stimulates proliferation in various cell types including oligodendrocyte precursor (Ackerman et al., 2015), cortical progenitor (Bae et al., 2014) and fibroblasts (Ke et al., 2007) cells. Here we show loss of *Gpr56* decreases 3T3-L1 cell proliferation. Reduced cell adhesion inhibits adipogenesis (Gabrielli et al., 2018)(Luo et al., 2008)(Kamiya et al., 2002) and GPR56 is a member of the adhesion GPCR family that is involved in adhesion of various cell types including developing neurons, haemopoietic stem cells and tumor cells (Shashidhar et al., 2005) (Koirala et al., 2009) (Yusuke et al., 2015). Here we show loss of *Gpr56* reduces cell adhesion. Bioinformatics show cell ECM is one of the pathways commonly dysregulated in

both human and mouse obese adipose tissue (Berger et al., 2015). Changes to ECM components including increased fibronectin or inhibition of collagen synthesis suppresses adipogenesis (Kamiya et al., 2002)(Liu et al., 2017). GPR56 expression is associated with changes in deposition of the ECM glycoprotein fibronectin (Millar et al., 2018). Here we show elevated *Fn1*, *Col1 $\alpha$ 1*, *Col3 $\alpha$ 1* and *Col4 $\alpha$ 1* gene transcripts are all observed in *Gpr56*<sup>-/-</sup> cells suggesting changes to ECM composition. The coordinated disruption of actin stress fibres is a prerequisite for adipogenesis (Nobusue et al., 2014). Enforced expression of GPR56 induces Rho-dependent actin stress fibres in NIH3T3 cells (Iguchi et al., 2008). Here we show *Gpr56*<sup>-/-</sup> cells already have significantly reduced actin stress fibres prior to stimulation with differentiation signals.

Our results show that the consequences of loss of Gpr56 directly or indirectly changes several properties that are all likely to contribute to inhibition of 3T3-L1 cell adipogenesis (summarised in Fig. 8). The normal role of GPR56 in regulating adipogenesis is unclear from these studies but we hypothesise that it may be related to its well characterised roles in cell adhesion and actin stress fibre formation (Shashidhar et al., 2005)(Koirala et al., 2009)(Yusuke et al., 2015)(Iguchi et al., 2008). It is well established that morphological changes from fibroblast like to rounded cells occur in differentiation of adipocytes (Smas & Sul, 2005) and this depends on both a reduction in cell adhesion and actin cytoskeleton reorganization. Premature actin cytoskeleton reorganization inhibits adipogenesis but if coordinated with standard differentiation signals, enhances the process (Titushkin et al., 2013). Our results suggest GPR56 is necessary for the formation of actin stress fibres in preadipocytes as they are dramatically reduced in *Gpr56*<sup>-/-</sup> cells. When preadipocytes are stimulated to differentiate Gpr56 expression declines which could result in the reduction of actin stress fibres allowing actin cytoskeleton reorganisation to occur enabling differentiation to proceed. This model suggests that Gpr56 regulates early stages of differentiation, consistent with the KD studies. Our results also show that Gpr56 levels recover after an initial decline in the adipocyte developmental programme. This suggests Gpr56 may also have a role at later stages of differentiation as well. Further studies are required to investigate this possibility.

Stable enforced expression of Gpr56 enhances proliferation and adhesion and moderately suppresses adipogenesis, causing reduced levels of Ppar $\gamma$ <sub>2</sub>, C/ebp $\alpha$ , Ap2 and Oil red O staining (Hasan and Bartholomew, unpublished). The reduced adipogenesis associated with increased Gpr56 expression *in vitro* correlates with the inverse relationship seen with *gpr56*

expression in adipose tissue and weight gain *in vivo* in lean vs obese Zucker rats . It is possible that changes to the same cell properties described for Gpr56<sup>-/-</sup> cells also contribute to suppression of adipogenesis observed with enforced expression although the effect is less severe. The observation that both increased and decreased Gpr56 expression reduce adipogenesis in 3T3-L1 cells suggests that both agonists and antagonists of this G-protein coupled receptor could affect the development of adipocytes.

In summary, this investigation shows that *GPR56* transcripts are reduced in adipose tissue of obese rodents and *in vitro* studies show that both enforced expression and loss of expression in 3T3-L1 cells suppress adipogenesis. Loss of Gpr56 has the greatest effect on the adipogenic developmental program. These studies suggest modulation of this protein and/or its biological activity could represent a target for development of novel therapeutic strategies for intervention in the treatment of obesity.

## References

- Abbott, D. W., & Holt, J. T. (1997). Finkel-Biskis-Reilly osteosarcoma virus v-Fos inhibits adipogenesis and both the activity and expression of CCAAT/enhancer binding protein  $\alpha$ , a key regulator of adipocyte differentiation. *Journal of Biological Chemistry*, 272(51), 32454–32462. <https://doi.org/10.1074/jbc.272.51.32454>
- Ackerman, S. D., Garcia, C., Piao, X., Gutmann, D. H., & Monk, K. R. (2015). The adhesion GPCR Gpr56 regulates oligodendrocyte development via interactions with G $\alpha$ 12/13 and RhoA. *Nature Communications*, 6(May 2014), 6122. <https://doi.org/10.1038/ncomms7122>
- Amisten, S., Neville, M., Hawkes, R., Persaud, S. J., Karpe, F., & Salehi, A. (2015). An atlas of G-protein coupled receptor expression and function in human subcutaneous adipose tissue. *Pharmacology & Therapeutics*, 146, 61–93. <https://doi.org/10.1016/j.pharmthera.2014.09.007>
- Aust, G., Zhu, D., Van Meir, E. G., & Xu, L. (2016). Adhesion GPCRs in Tumorigenesis. *Handbook of Experimental Pharmacology*, 234, 369–396. [https://doi.org/10.1007/978-3-319-41523-9\\_17](https://doi.org/10.1007/978-3-319-41523-9_17)
- Bae, B.-I., Tietjen, I., Atabay, K. D., Evrony, G. D., Johnson, M. B., Asare, E., ... Walsh, C. A. (2014). Evolutionarily Dynamic Alternative Splicing of GPR56 Regulates Regional Cerebral Cortical Patterning. *Science*, 343(6172), 764 LP – 768. <http://science.sciencemag.org/content/343/6172/764.abstract>
- Bannai, Y., Aminova, L. R., Faulkner, M. J., Ho, M., & Wilson, B. A. (2012). Rho/ROCK-dependent inhibition of 3T3-L1 adipogenesis by G-protein-deamidating dermonecrotic toxins: differential regulation of Notch1, Pref1/Dlk1, and  $\beta$ -catenin signaling. *Frontiers in Cellular and Infection Microbiology*, 2(June), 80. <https://doi.org/10.3389/fcimb.2012.00080>
- Berger, E., Héraud, S., Mojallal, A., Lequeux, C., Weiss-Gayet, M., Damour, O., & Géloën, A. (2015). Pathways commonly dysregulated in mouse and human obese adipose tissue: FAT/CD36 modulates differentiation and lipogenesis. *Adipocyte*, 4(3), 161–180. <https://doi.org/10.4161/21623945.2014.987578>
- Cao, Z., Umek, R. M., & McKnight, S. L. (1991). Regulated expression of three C/EBP

isoforms during adipose conversion of 3T3-L1 cells. *Genes & Development*, 5(9), 1538–1552. Retrieved from <http://www.ncbi.nlm.nih.gov/pubmed/1840554>

Duner, P., Al-Amily, I. M., Soni, A., Asplund, O., Safi, F., Storm, P., ... Salehi, A. (2016). Adhesion G Protein-Coupled Receptor G1 (ADGRG1/GPR56) and Pancreatic beta-Cell Function. *The Journal of Clinical Endocrinology and Metabolism*, 101(12), 4637–4645. <https://doi.org/10.1210/jc.2016-1884>

Eisenstein, A. (2013). G Protein-Coupled Receptors and Adipogenesis : A Focus on Adenosine Receptors, (September), 414–421. <https://doi.org/10.1002/jcp.24473>

Farmer, S. R. (2006). Transcriptional control of adipocyte formation. *Cell Metabolism*, 4(4), 263–273. <https://doi.org/10.1016/j.cmet.2006.07.001>

Gabrielli, M., Romero, D. G., Martini, C. N., Raiger Iustman, L. J., & Vila, M. D. C. (2018). MCAM knockdown impairs PPARgamma expression and 3T3-L1 fibroblasts differentiation to adipocytes. *Molecular and Cellular Biochemistry*, 448(1–2), 299–309. <https://doi.org/10.1007/s11010-018-3334-8>

Heath, V. J., Gillespie, D. A., & Crouch, D. H. (2000). Inhibition of the terminal stages of adipocyte differentiation by cMyc. *Experimental Cell Research*, 254(1), 91–98. <https://doi.org/10.1006/excr.1999.4736>

Hu, E., Kim, J. B., Sarraf, P., & Spiegelman, B. M. (1996). Inhibition of adipogenesis through MAP kinase-mediated phosphorylation of PPARgamma. *Science (New York, N.Y.)*, 274(5295), 2100–2103.

Iguchi, T., Sakata, K., Yoshizaki, K., Tago, K., Mizuno, N., & Itoh, H. (2008). Orphan G Protein-coupled Receptor GPR56 Regulates Neural Progenitor Cell Migration via a G 12/13 and Rho Pathway. *Journal of Biological Chemistry*, 283(21), 14469–14478. <https://doi.org/10.1074/jbc.M708919200>

Kamiya, S., Kato, R., Wakabayashi, M., Tohyama, T., Enami, I., Ueki, M., ... Fukai, F. (2002). Fibronectin peptides derived from two distinct regions stimulate adipocyte differentiation by preventing fibronectin matrix assembly. *Biochemistry*, 41(9), 3270–3277.

Ke, N., Sundaram, R., Liu, G., Chionis, J., Fan, W., Rogers, C., ... Li, Q.-X. (2007). Orphan G protein-coupled receptor GPR56 plays a role in cell transformation and tumorigenesis involving the cell adhesion pathway. *Molecular Cancer Therapeutics*, 6(6), 1840–1850. <https://doi.org/10.1158/1535-7163.MCT-07-0066>

Koirala, S., Jin, Z., Piao, X., & Corfas, G. (2009). GPR56-regulated granule cell adhesion is essential for rostral cerebellar development. *The Journal of Neuroscience : The Official Journal of the Society for Neuroscience*, 29(23), 7439–7449. <https://doi.org/10.1523/JNEUROSCI.1182-09.2009>

Liu, C., Huang, K., Li, G., Wang, P., Liu, C., Guo, C., ... Pan, J. (2017). Ascorbic acid promotes 3T3-L1 cells adipogenesis by attenuating ERK signaling to upregulate the collagen VI. *Nutrition and Metabolism*, 14(1), 1–12. <https://doi.org/10.1186/s12986-017-0234-y>

Livak, K. J., & Schmittgen, T. D. (2001). Analysis of relative gene expression data using real-time quantitative PCR and the 2(-Delta Delta C(T)) Method. *Methods (San Diego, Calif.)*, 25(4), 402–408. <https://doi.org/10.1006/meth.2001.1262>

Luo, R., Jeong, S.-J., Jin, Z., Strokes, N., Li, S., & Piao, X. (2011, August 2). G protein-coupled receptor 56 and collagen III, a receptor-ligand pair, regulates cortical development and lamination. *Proceedings of the National Academy of Sciences of the United States of America*. <https://doi.org/10.1073/pnas.1104821108>

Luo, W., Shitaye, H., Friedman, M., Bennett, C. N., Miller, J., MacDougald, O. A., & Hankenson, K. D. (2008). Disruption of cell–matrix interactions by heparin enhances mesenchymal progenitor adipocyte differentiation. *Experimental Cell Research*,

314(18), 3382–3391. <https://doi.org/10.1016/j.yexcr.2008.07.003>

Mali, P., Yang, L., Esvelt, K. M., Aach, J., Guell, M., James, E., ... Church, G. M. (2013). RNA-Guided Human Genome Engineering via Cas9. *Science*, 339(6121), 823–826. <https://doi.org/10.1126/science.1232033>.

Mehta, P., & Piao, X. (2017). Adhesion G-protein coupled receptors and extracellular matrix proteins: Roles in myelination and glial cell development. *Developmental Dynamics*, 246(4), 275–284. <https://doi.org/10.1002/dvdy.24473>

Millar, M. W., Corson, N., & Xu, L. (2018). The Adhesion G-Protein-Coupled Receptor, GPR56/ADGRG1, Inhibits Cell-Extracellular Matrix Signaling to Prevent Metastatic Melanoma Growth. *Frontiers in Oncology*, 8(February), 8. <https://doi.org/10.3389/fonc.2018.00008>

Myneni, V. D., Melino, G., & Kaartinen, M. T. (2015). Transglutaminase 2--a novel inhibitor of adipogenesis. *Cell Death & Disease*, 6, e1868. <https://doi.org/10.1038/cddis.2015.238>

Nobusue, H., Onishi, N., Shimizu, T., Sugihara, E., Oki, Y., Sumikawa, Y., ... Kano, K. (2014). Regulation of MKL1 via actin cytoskeleton dynamics drives adipocyte differentiation. *Nature Communications*, 5, 1–12. <https://doi.org/10.1038/ncomms4368>

Okamura, M., Kudo, H., Wakabayashi, K., Tanaka, T., Nonaka, A., Uchida, A., ... Sakai, J. (2009). COUP-TFII acts downstream of Wnt/beta-catenin signal to silence PPARgamma gene expression and repress adipogenesis. *Proceedings of the National Academy of Sciences of the United States of America*, 106(14), 5819–5824. <https://doi.org/10.1073/pnas.0901676106>

Papers, J. B. C., & Doi, M. (2007). Genetic and Pharmacological Inhibition of Rho-associated Kinase II Enhances Adipogenesis \*, 282(40), 29574–29583. <https://doi.org/10.1074/jbc.M705972200>

Piao, X., Hill, R. S., Bodell, A., Chang, B. S., Basel-Vanagaite, L., Strausberg, R., ... Walsh, C. A. (2004). G protein-coupled receptor-dependent development of human frontal cortex. *Science (New York, N.Y.)*, 303(5666), 2033–2036. <https://doi.org/10.1126/science.1092780>

Rao, T. N., Marks-Bluth, J., Sullivan, J., Gupta, M. K., Chandrakanthan, V., Fitch, S. R., ... Wagers, A. J. (2015). High-level Gpr56 expression is dispensable for the maintenance and function of hematopoietic stem and progenitor cells in mice. *Stem Cell Research*, 14(3), 307–322. <https://doi.org/10.1016/j.scr.2015.02.001>

Rosen, E. D., Hsu, C.-H., Wang, X., Sakai, S., Freeman, M. W., Gonzalez, F. J., & Spiegelman, B. M. (2002). C/EBPalpha induces adipogenesis through PPARgamma: a unified pathway. *Genes & Development*, 16(1), 22–26. <https://doi.org/10.1101/gad.948702>

Ross, S. E., Hemati, N., Longo, K. A., Bennett, C. N., Lucas, P. C., Erickson, R. L., & MacDougald, O. A. (2000). Inhibition of Adipogenesis by Wnt Signaling. *Science*, 289(5481), 950 LP – 953. Retrieved from <http://science.sciencemag.org/content/289/5481/950.abstract>

Saito, Y., Kaneda, K., Suekane, A., Ichihara, E., Nakahata, S., Yamakawa, N., ... Morishita, K. (2013). Maintenance of the hematopoietic stem cell pool in bone marrow niches by EVI1-regulated GPR56. *Leukemia*, 27(8), 1637–1649. <https://doi.org/10.1038/leu.2013.75>

Saito, Yusuke, & Morishita, K. (2015). Maintenance of leukemic and normal hematopoietic stem cells in bone marrow niches by EVI1-regulated GPR56. *The Japanese Journal of Clinical Hematology*, 56(4), 375–383. <https://doi.org/10.11406/rinketsu.56.375>

Schroeder-Gloeckler, J. M., Rahman, S. M., Janssen, R. C., Qiao, L., Shao, J., Roper, M., ... Friedman, J. E. (2007). CCAAT/enhancer-binding protein beta deletion reduces adiposity, hepatic steatosis, and diabetes in Lepr(db/db) mice. *The Journal of Biological*

*Chemistry*, 282(21), 15717–15729. <https://doi.org/10.1074/jbc.M701329200>

Shashidhar, S., Lorente, G., Nagavarapu, U., Nelson, A., Kuo, J., Cummins, J., ... Foehr, E. D. (2005). GPR56 is a GPCR that is overexpressed in gliomas and functions in tumor cell adhesion. *Oncogene*, 24(10), 1673–1682. <https://doi.org/10.1038/sj.onc.1208395>

Smas, C. M., & Sul, H. S. (2015). Control of adipocyte differentiation. *Biochemical Journal*, 309(3), 697–710. <https://doi.org/10.1042/bj3090697>

Spaethling, J. M., Sanchez-Alavez, M., Lee, J. H., Xia, F. C., Dueck, H., Wang, W., ... Eberwine, J. (2016). Single-cell transcriptomics and functional target validation of brown adipocytes show their complex roles in metabolic homeostasis. *FASEB Journal*, 30(1), 81–92. <https://doi.org/10.1096/fj.15-273797>

Stoscheck, C. M. (1990). [6] Quantitation of protein. *Methods in Enzymology*, 182, 50–68. [https://doi.org/10.1016/0076-6879\(90\)82008-P](https://doi.org/10.1016/0076-6879(90)82008-P)

Titushkin, I., Sun, S., Paul, A., & Cho, M. (2013). Control of adipogenesis by ezrin, radixin and moesin-dependent biomechanics remodeling. *Journal of Biomechanics*, 46(3), 521–526. <https://doi.org/10.1016/j.jbiomech.2012.09.027>

Todaró, G. J. & Green, H. (1963). Quantitative studies of the growth of mouse embryo cells in culture and their development into established lines. *Journal of Cell Biology*, 17, 299–313.

Tontonoz, P., Graves, R. a, Budavari, a I., Erdjument-Bromage, H., Lui, M., Hu, E., ... Spiegelman, B. M. (1994). Adipocyte-specific transcription factor ARF6 is a heterodimeric complex of two nuclear hormone receptors, PPAR gamma and RXR alpha. *Nucleic Acids Research*, 22(25), 5628–5634.

White, J. P., Wrann, C. D., Rao, R. R., Nair, S. K., Jedrychowski, M. P., You, J.-S., ... Spiegelman, B. M. (2014). G protein-coupled receptor 56 regulates mechanical overload-induced muscle hypertrophy. *Proceedings of the National Academy of Sciences*, 111(44), 15756–15761. <https://doi.org/10.1073/pnas.1417898111>

Xu, L., Begum, S., Hearn, J. D., & Hynes, R. O. (2006). GPR56, an atypical G protein-coupled receptor, binds tissue transglutaminase, TG2, and inhibits melanoma tumor growth and metastasis. *Proceedings of the National Academy of Sciences of the United States of America*, 103(24), 9023–9028. <https://doi.org/10.1073/pnas.0602681103>

## Figure legends

**Fig.1** *GPR56* gene expression in rodent adipose tissue and 3T3-L1 cells. **A** Reverse-transcription quantitative real-time polymerase chain reaction (QPCR) analysis of *gpr56* gene expression, normalized to *gapdh*, in lean (black bars) and obese (white bars) male Zucker rat abdominal visceral white adipose tissue. Histograms are the mean gene expression ( $2\Delta^{Ct}$ ) from 6 animals (n=6). Statistical analysis shows unpaired two-tailed Student t-test of lean vs obese animals, \*\*\* $p \leq 0.001$ . **B** Shows confocal images of  $\alpha$ -GPR56 (green) immuno-stained 3T3-L1 cells. Non-permeabilised and permeabilised cells are indicated by – and + respectively. Control cells are stained with  $\alpha$ -Vesicular stomatitis virus G protein epitope (VSVG) isotype matched and secondary antibodies or secondary antibody only as indicated. Merged images show both immuno- and DAPI (blue) stain. White size bar is either 20 $\mu$ m (+) or 5 $\mu$ m (-). **C** Histogram showing semi-quantitative analysis of Oil Red O staining of 3T3-L1 cells at indicated days following induction of differentiation, n=3. Statistical analysis shows one-way ANOVA and Dunnett's multiple comparisons test relative to day 0 \*\*\*\* $p \leq 0.0001$ . **D** QPCR analysis of *Gpr56*, normalized to *18S* rRNA, at indicated days following induction of differentiation of 3T3-L1 cells. Histogram shows mean expression relative to gene at day 0, which is used as calibrator, n=3. Statistical analysis shows one-way ANOVA and Dunnett's multiple comparisons test relative to day 0 \*\* $p \leq 0.01$ . All error bars show standard error of mean.

**Fig.2** *Gpr56* knockdown in 3T3-L1 cells. **A** Schematic representation of murine *Gpr56* gene exons. Exons are indicated by rectangles and coding exons are shaded. Exon numbers are indicated for exons 1, 3, 11 and 14 (Ex1, Ex3, Ex11, Ex14) only. The start codon is represented by ATG and approximate target regions for DsiRNAs 1, 2 and 3 indicated by grey shading. Also shown are the target sequences for guide RNA plasmid vectors pCW2 and pRM4, which are located in exon 3. Protospacer adjacent motif (PAM) sequences are underlined. **B** Reverse-transcription quantitative real-time polymerase chain reaction analysis of *Gpr56* gene expression in 3T3-L1 cells treated with either control S. siRNA or test G-DsiRNA 2 at the indicated day of differentiation. Histograms show mean gene expression of 3 independent experiments normalized to *18S* rRNA relative to gene expression of *Gpr56* (*Gpr56F* & *R* primers) in control S. siRNA treated cells at day 0 as calibrator. Error bars show standard error of mean, n=3. Statistical analysis shows multiple t test, significance determined using the Holm-Sidak method of S. siRNA vs G-DsiRNA 2 each day, \*\*  $p \leq 0.01$ ,

\*\*\*  $p \leq 0.001$ . **C** Confocal images of  $\alpha$ -GPR56 (green) immuno-stained permeabilized control S. siRNA and G-DsiRNA 2 treated 3T3-L1 cells. Merged images show both immuno- and DAPI (blue) stain. White size bar is 20 $\mu$ m.

**Fig.3** Adipogenesis in *Gpr56* knockdown 3T3-L1 cells using G-DsiRNA 2. **A** Semi-quantitative analysis of Oil Red O stained 3T3-L1 cells at days 0, 4 and 10 of differentiation, following treatment with or without (C) the indicated scrambled control (S. siRNA) or *Gpr56* (G-DsiRNA2) siRNA's. Histogram is the mean value of three independent experiments and the error bars the standard error of mean. Statistical analysis shows two-way ANOVA and Dunnett's multiple comparisons test of S. siRNA vs Control (C) and G-DsiRNA 2 vs Control (C), \*  $p \leq 0.05$ , \*\*\*  $p \leq 0.01$ . **B** Typical western blot of S. siRNA or G-DsiRNA2 treated cells at days 0, 4 and 10 of differentiation with the indicated antibodies. Specific proteins of the expected size are indicated by black line.

**Fig.4** Partial nucleotide sequence of *Gpr56* gene alleles in 3T3-L1 genome edited cells, using single letter code. Only sequence of the pCW2 and pRM4 gRNA target regions and adjacent protospacer adjacent motif (underlined) are shown. WT depicts the normal wildtype sequence for murine *Gpr56*. Sequence shown in bold indicates deleted nucleotides of mutant alleles. CW and RM indicates nucleotide sequence of independently cloned DNA fragments derived from *Gpr56* with – highlighting deleted region. Sequence of eight and seven independent recombinant DNA clones derived from cell clone CW2.2.4 and RM4.2.5.5 DNA respectively are shown. \* indicates regions of identity between WT and CW or RM derived DNA. In both cases sequence of two distinct alleles only are seen and the size of deletion ( $\Delta$ ) of each allele is shown. Below the single letter nucleotide sequence are chromatograms of DNA sequence of this region for all *Gpr56* alleles presented.

**Fig.5** Adipogenesis in *Gpr56* genome edited 3T3-L1 cells. **A** Oil Red O stained 3T3-L1 and genome edited CW2.2.4 and RM4.2.5.5 cells at days 0, 4 and 10 semi-quantified by absorbance at 492nm. Histogram is the mean value of three independent experiments and the error bars the standard error of mean. Statistical analysis shows two-way ANOVA and Dunnett's multiple comparisons test of 3T3-L1 vs CW2.2.4 or RM4.2.5.5 for each induction day, \*\*  $p \leq 0.01$ , \*\*\*  $p \leq 0.001$ . **B** Typical Western blot of 3T3-L1 or RM4.2.5.5 cells at days



0, 4 and 10 of differentiation with the indicated antibodies. Specific proteins of the expected size are indicated by black line.

**Fig.6** Characterisation of proliferation, adhesion and extracellular matrix gene expression in *Gpr56* genome edited 3T3-L1 cells **A** Proliferation of the indicated cell lines over the period of days shown. Histogram shows the mean of three independent experiments, n=3. Statistical analysis shows two-way ANOVA and Dunnett's multiple comparisons test of 3T3-L1 vs either RM4.2.5.5 or CW2.2.4, \*  $p \leq 0.05$ , \*\*  $p \leq 0.01$ , \*\*\*  $p \leq 0.001$ , \*\*\*\*  $p \leq 0.0001$ .

**B** Crystal violet stained adherent cells for the indicated cell lines, quantified by absorbance at 570nm. Histogram shows the mean of three independent experiments, n=3. Statistical analysis shows one-way ANOVA and Dunnett's multiple comparison test of 3T3-L1 vs either RM4.2.5.5 or CW2.2.4, \*  $p \leq 0.05$ , \*\*  $p \leq 0.01$ . **C** Reverse-transcription quantitative real-time polymerase chain reaction analysis of indicated gene expression in 3T3-L1 and RM4.2.5.5 cells at days 0 and 10 of differentiation. Histograms show mean gene expression of 3 independent experiments normalized to 18S rRNA relative to expression of the same gene in 3T3-L1 cells at day 0 as calibrator, n=3. Statistical analysis by two-way ANOVA and Sidak's multiple comparisons test of 3T3-L1 vs RM4.2.5.5 cells for each induction day, \*  $p \leq 0.05$ , \*\*  $p \leq 0.01$ , \*\*\*  $p \leq 0.001$ , \*\*\*\*  $p \leq 0.0001$ . All error bars show standard error of mean.

**Fig.7 A** Confocal images of Phalloidin staining of actin cytoskeleton in 3T3-L1 and RM4.2.5.5 cells. Actin is stained with iFlour 488 conjugated Phalloidin (green). Merged images show both Phalloidin and DAPI (blue) stain. White arrows indicate regions selected for magnification shown in adjacent panels. The white size lines indicate scale bar of 20 $\mu$ m or 10 $\mu$ m. **B** Histogram showing quantitative analysis of Phalloidin stained confocal images of the indicated cell lines using ImageJ software. Statistical analysis shows unpaired Student t test, \*\*  $p \leq 0.01$ .

**Fig.8** Model illustrating adipogenesis in *Gpr56* +ve and -ve cells. Model shows the cell membrane lipid bilayer and *Gpr56* transmembrane protein (+ve *Gpr56*) indicated by a black line passing through membrane that is absent in *Gpr56* -ve cells (-ve *Gpr56*). Chemical treatment of preadipocytes allows induction of *Ppar $\gamma$ 2* and *C/ebp $\alpha$*  in the presence (+ve *Gpr56*) but not absence (-ve *Gpr56*) of *Gpr56*. Differentiation is indicated by morphological change from spindle like preadipocyte fibroblast cells to round adipocyte which occurs in the

presence of Gpr56 (indicated by solid arrow) and maintenance of the fibroblast like morphology is blocked (indicated by broken arrow). The link between Gpr56 and +ve stimulation of adipogenesis is unknown and indicated by ?. In the absence of Gpr56 the change from fibroblast to adipocyte cells is blocked (broken arrow) and cells remain fibroblast like (solid arrow). In the absence of Gpr56 several possible mechanisms are proposed to inhibit Ppar $\gamma_2$ /C/ebp $\alpha$  production (down arrow) and differentiation. Sustained levels of the known inhibitor of Ppar $\gamma_2$  (black line) and adipogenesis, active  $\beta$ -catenin, is increased (up arrow). Reduced cell proliferation, adhesion and actin cytoskeleton (down arrows) and changes in extracellular matrix (ECM) gene expression, that result from loss of Gpr56, are all proposed to contribute to inhibition of adipogenesis (indicated by broken lines).

### Supplementary Figure Legends

**S1** Gpr56 knockdown in 3T3-L1 cells. **A** Reverse-transcription quantitative real-time polymerase chain reaction analysis of *Gpr56* gene expression in 3T3-L1 cells treated with the indicated DsiRNA's. Histograms show mean gene expression of 3 independent DsiRNA treated cells normalized to 18S rRNA relative to expression of *Gpr56* in untreated 3T3-L1 cells as calibrator, n=3. Statistical analysis shows one-way ANOVA and Dunnett's multiple comparisons test of control (C) vs DsiRNA treated cells, \*\*  $p \leq 0.01$ , \*\*\*\*  $p \leq 0.0001$ . **B** Quantitative analysis of the indicated Gpr56 immuno-stained confocal cell images using ImageJ software. Statistical analysis shows unpaired two tailed Student t test, \*\*  $p \leq 0.01$ . **C** Example of typical image of Oil Red O stained 3T3-L1 non-transfected control (NTC), scrambled siRNA (S. siRNA) and Gpr56 siRNA (DsiRNA 2) treated cells at the indicated days of differentiation. **D** Quantitative analysis of Western blot with indicated antibodies relative to REVERT<sup>TM</sup> (LiCoR) total cellular protein stain. Histograms are the mean band intensity for three independent scrambled control (S. siRNA) or *Gpr56* siRNA (G-DsiRNA2) treated cells at days 0, 4 and 10 with the indicated antibodies, n=3. Statistical analysis shows two-way ANOVA and Sidak's multiple comparisons test of S.siRNA vs G-DsiRNA2, \*  $p \leq 0.05$ , \*\*  $p \leq 0.01$ , \*\*\*\*  $p \leq 0.001$ . All error bars show standard error of mean.

**S2** Adipogenesis of Gpr56 knockdown 3T3-L1 cells using G-DsiRNA 1. Oil Red O stained 3T3-L1 cells at days 0, 4 and 10 semi-quantified by absorbance at 492nm, following treatment with or without (C) the indicated siRNA's. Histogram is the mean value of three

independent experiments and the error bars the standard error of mean. Statistical analysis shows two-way ANOVA and Dunnett's multiple comparison test of untreated (C) vs control siRNA (S.siRNA) or untreated vs *Gpr56* siRNA (G-DsiRNA1), (\*\*\*)  $p \leq 0.001$ .

**S3** Profile of *Ppar $\gamma$ <sub>2</sub>* and *Ap2* gene expression during adipogenesis of G-DsiRNA 2 treated 3T3-L1 cells. Reverse-transcription quantitative real-time polymerase chain reaction analysis of indicated gene expression in 3T3-L1 siRNA control (S.siRNA, black bars) siRNA *Gpr56* (G-DsiRNA 2, white bars) treated cells using *Ppar $\gamma$ <sub>2</sub>F*, *Ppar $\gamma$ <sub>2</sub>R*, *Ap2F* and *Ap2R* primers. Histograms show mean gene expression of 3 independently transfected 3T3-L1 cells with the indicated siRNA's normalized to *18S* rRNA relative to expression of the same gene in S.siRNA treated cells at day 0 as calibrator. Error bars show standard error of mean. Statistical analysis by two-way ANOVA and Sidak's multiple comparisons test of S.siRNA vs G-DsiRNA 2 treated cells for each induction day, \*  $p \leq 0.05$ , \*\*  $p \leq 0.01$ , \*\*\*  $p \leq 0.001$ .

**S4 A** Heteroduplex analysis of *Gpr56* genome edited cells showing examples of second and third round clones of CW and RM cells respectively. Analytical 0.8% agarose gel electrophoresis of either uncut (U) or heteroduplex analysis (T7) of polymerase chain reaction (PCR) amplified genomic DNA from the clones indicated. The expected size bands for PCR amplified DNA of 952bp and bacteriophage T7 endonuclease digested heteroduplex DNA (approx.. 743bp or 794bp) are indicated by arrows. Selected clones CW2.2.4 and RM4.2.5.5 are indicated by \*. M indicates molecular weight marker. **B** Confocal images of the indicated  $\alpha$ -GPR56 (green) immuno-stained permeabilized cells. Control cells are stained with secondary antibody only. Merged images show both immuno- and DAPI (blue) stain. White size bar is 20 $\mu$ m. **C** Histogram showing quantitative analysis of images using ImageJ software. Statistical analysis shows unpaired two tailed Student t test, \*\*\*\*  $p \leq 0.001$ .

**S5 A** Example of typical image of Oil Red O stained 3T3-L1 and *Gpr56* genome edited cells CW2.2.4 and RM4.2.5.5 at the indicated days (0, 4, 10) of differentiation. **B** Quantitation of regulator and marker proteins during adipogenesis of *Gpr56* genome edited cells. Quantitative analysis of Western blot with indicated antibodies relative to REVERT™ (LiCoR) total cellular protein stain. Histograms are the mean band intensity for three independent cultures of 3T3-L1 WT and RM4.2.5.5 cells at days 0, 4 and 10 with the

indicated antibodies. Statistical analysis shows two-way ANOVA and Sidak's multiple comparisons test of 3T3L1 vs RM4.2.5.5, \*\*  $p \leq 0.01$ , \*\*\*  $p \leq 0.001$ .

**S6 Optimisation of  $\beta$ -catenin KD and differentiation of RM4.2.5.5 cells.** **A** Reverse-transcription quantitative real-time polymerase chain reaction analysis of  $\beta$ -catenin gene expression ( $\beta$ -catenin F & R primers) in 3T3-L1 cells treated with the indicated DsiRNA's (Mixed indicates all three DsiRNA's). Histograms show mean gene expression of 3 independent DsiRNA treated cell cultures normalized to 18S rRNA relative to expression of  $\beta$ -catenin in untreated 3T3-L1 cells as calibrator, n=3. Statistical analysis shows one-way ANOVA and Dunnett's multiple comparisons test of control (C) vs DsiRNA treated cells, \*\*\*\*  $p \leq 0.0001$ . **B** Typical western blot of 3T3-L1 cells treated with indicated siRNA's with the indicated antibodies. Specific proteins of the expected size are indicated by black line. **C** Quantitative analysis of  $\beta$ -catenin WB relative to  $\beta$ -actin. Histograms are the mean band intensity for three independent cultures of 3T3-L1 cells treated with the indicated siRNA's. Statistical analysis shows unpaired Student t test, \*\*\*  $p \leq 0.001$ . **D** Oil Red O stained RM4.2.5.5 cells treated with the indicated siRNA's at days 0, 4 and 10 of differentiation, semi-quantified by absorbance at 492nm. Histogram is the mean value of three independent experiments, n=3. All error bars show standard error of mean.

#### **Conflict of Interest Statement:**

The authors have no conflicts of interest to declare

#### **Data sharing and data accessibility:**

The data that support the findings of this study are available from the corresponding author upon reasonable request.

#### **Author contribution statement:**

MAH, PR and SD performed the experimental work. MAH, CB, PEM and SP designed experiments and interpreted data. MAH and CB prepared the manuscript.

Fig.1

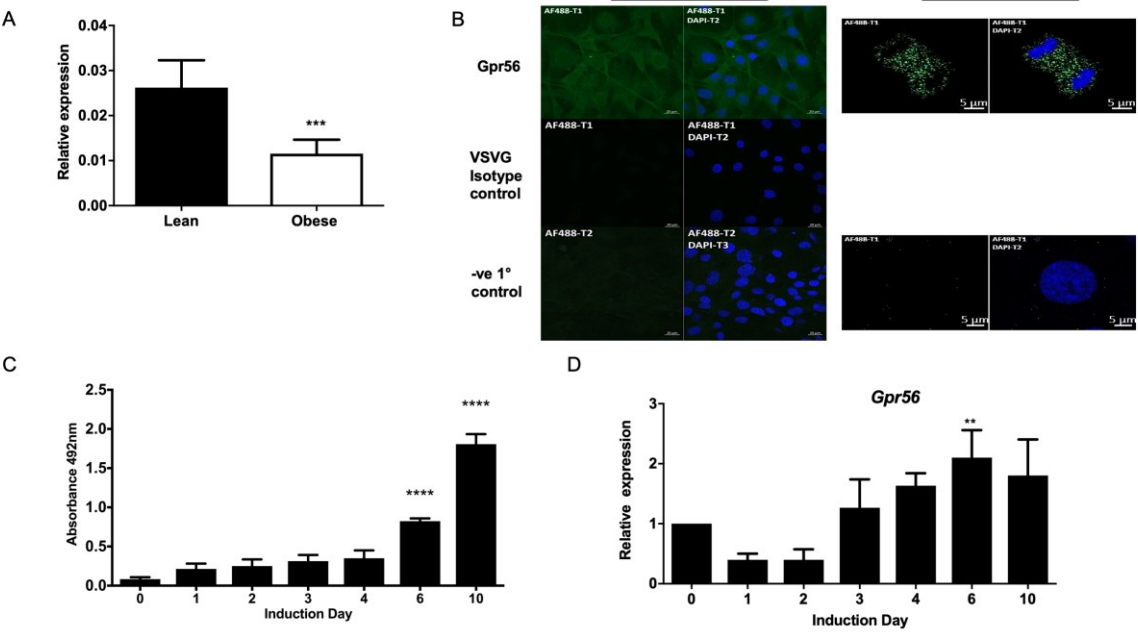


Fig.2

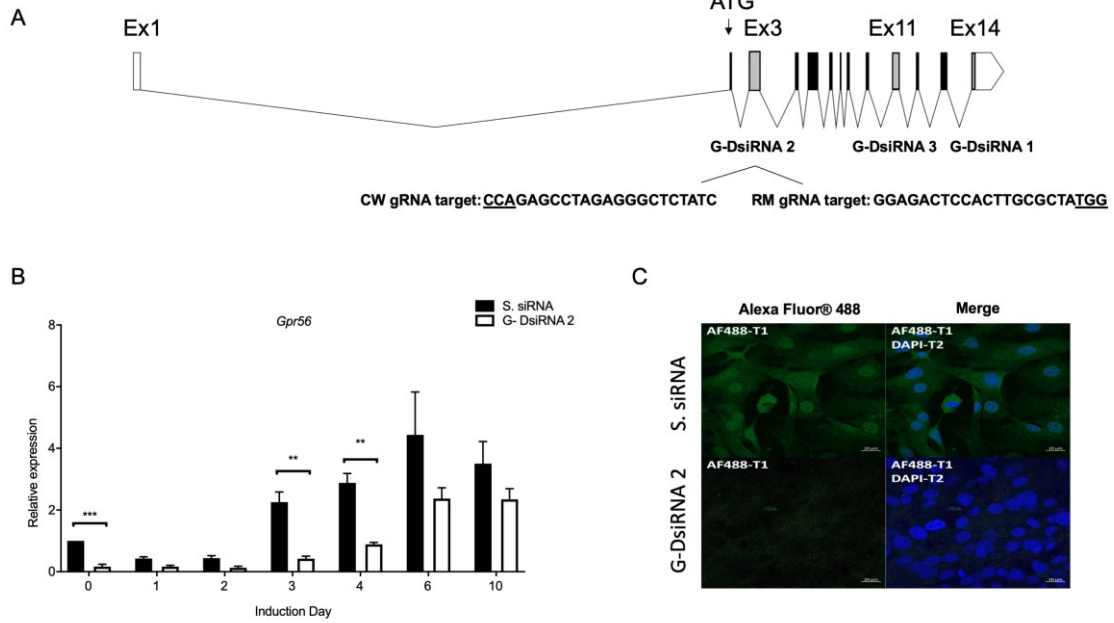
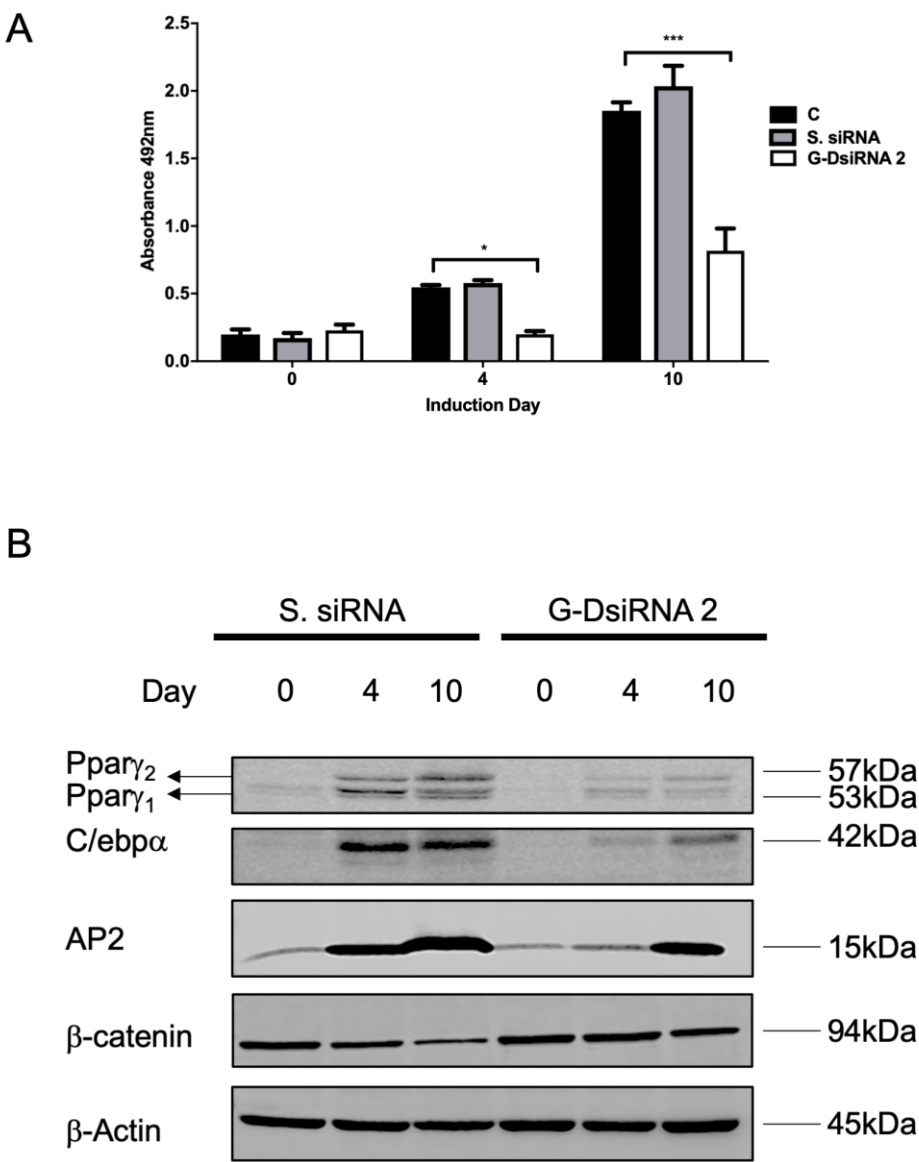
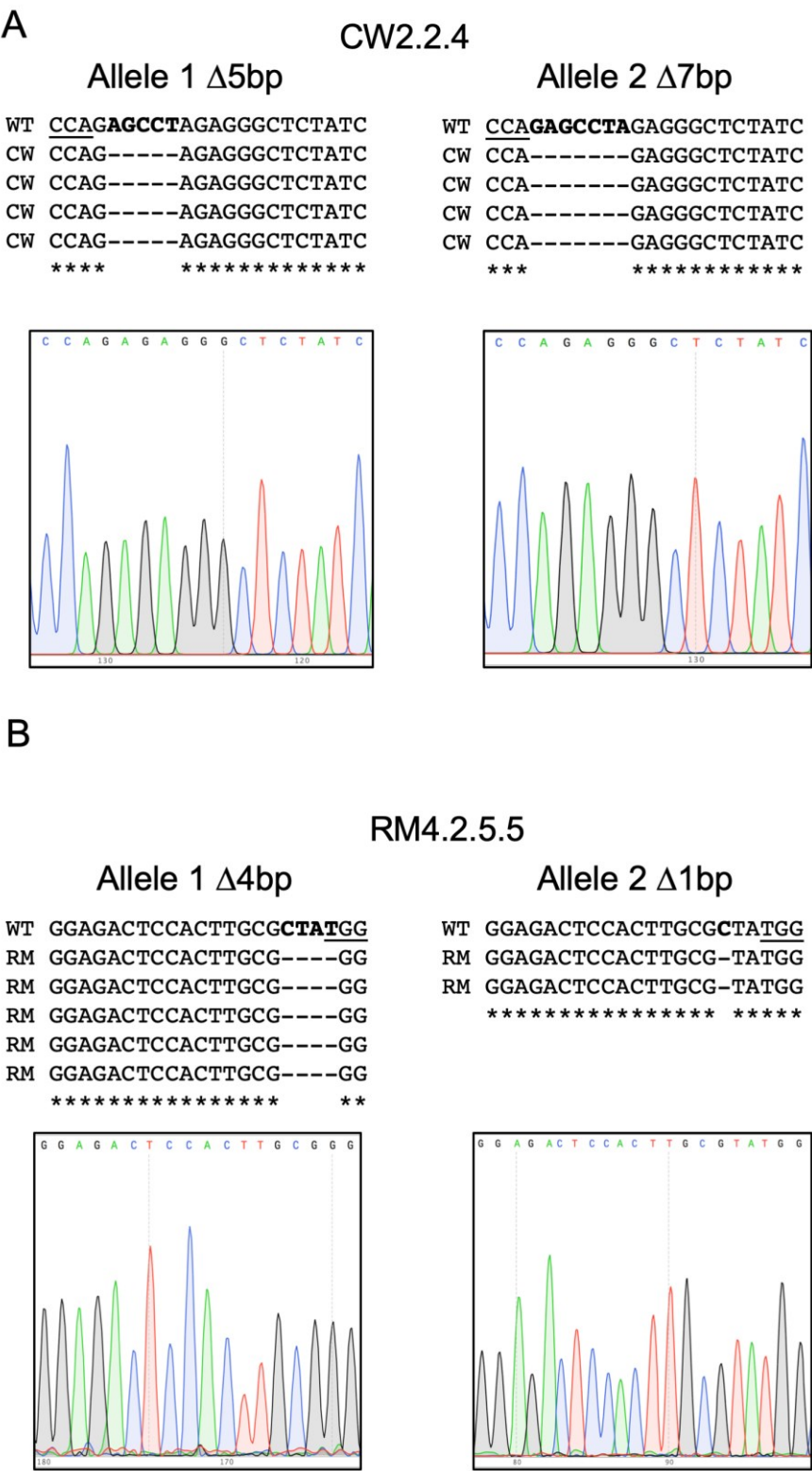


Fig.3



860  
861

Fig.4



862  
863

Fig.5

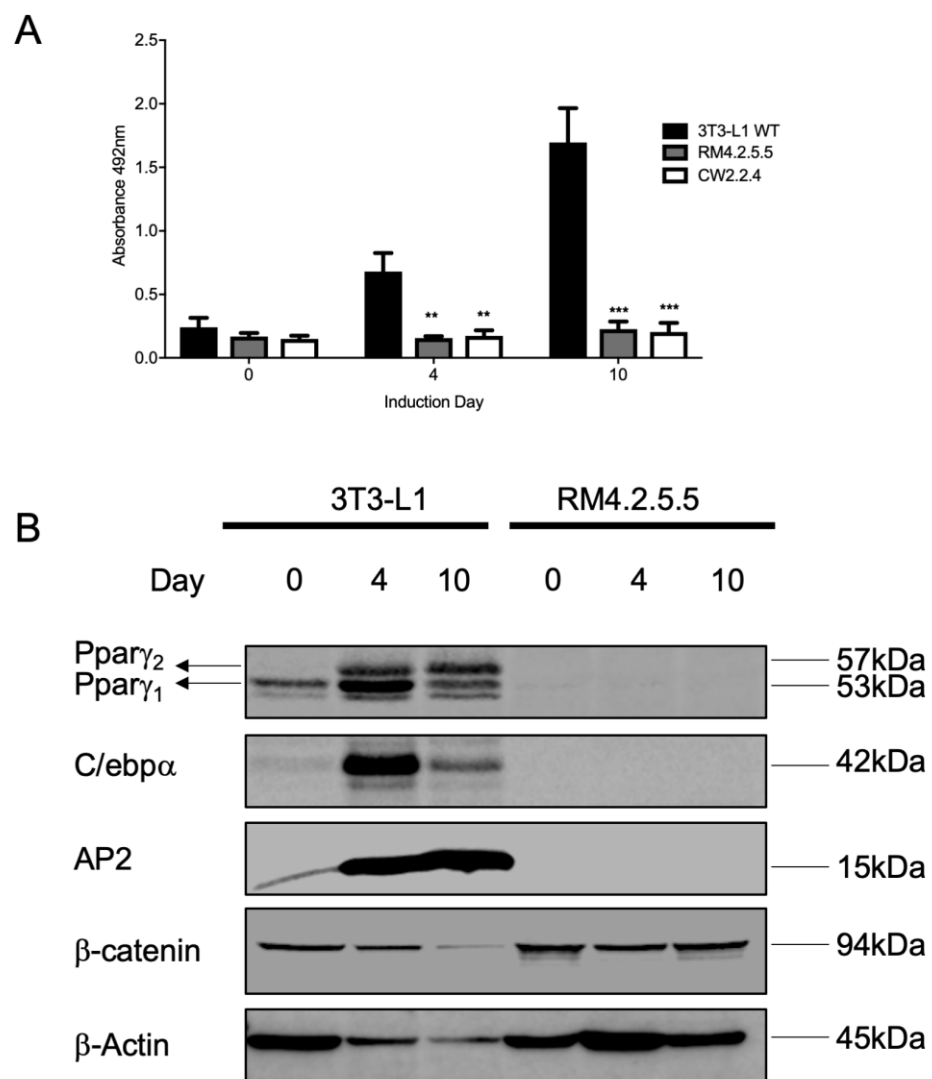
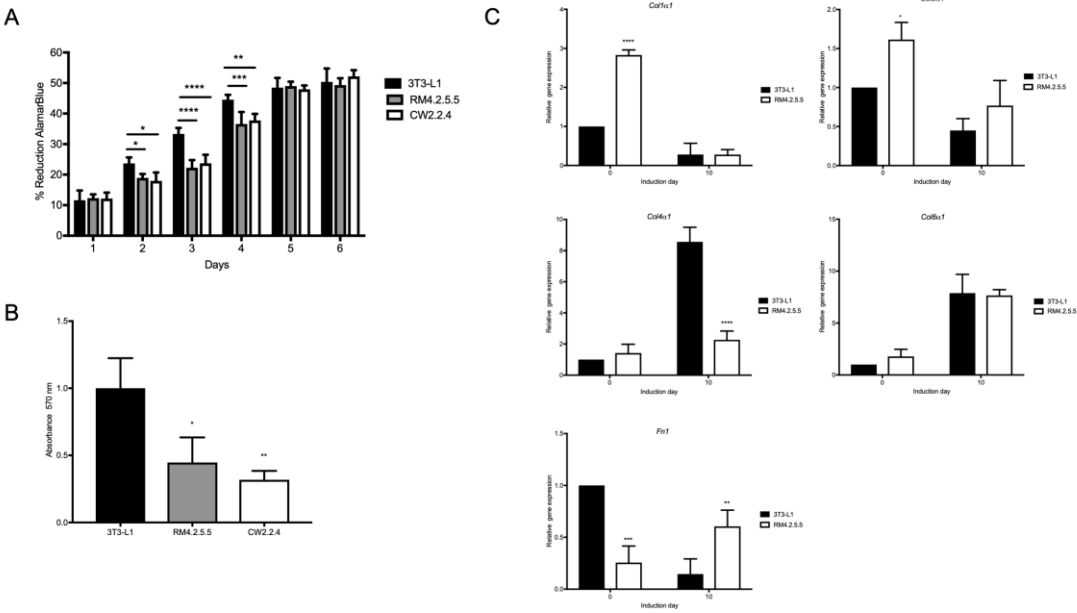




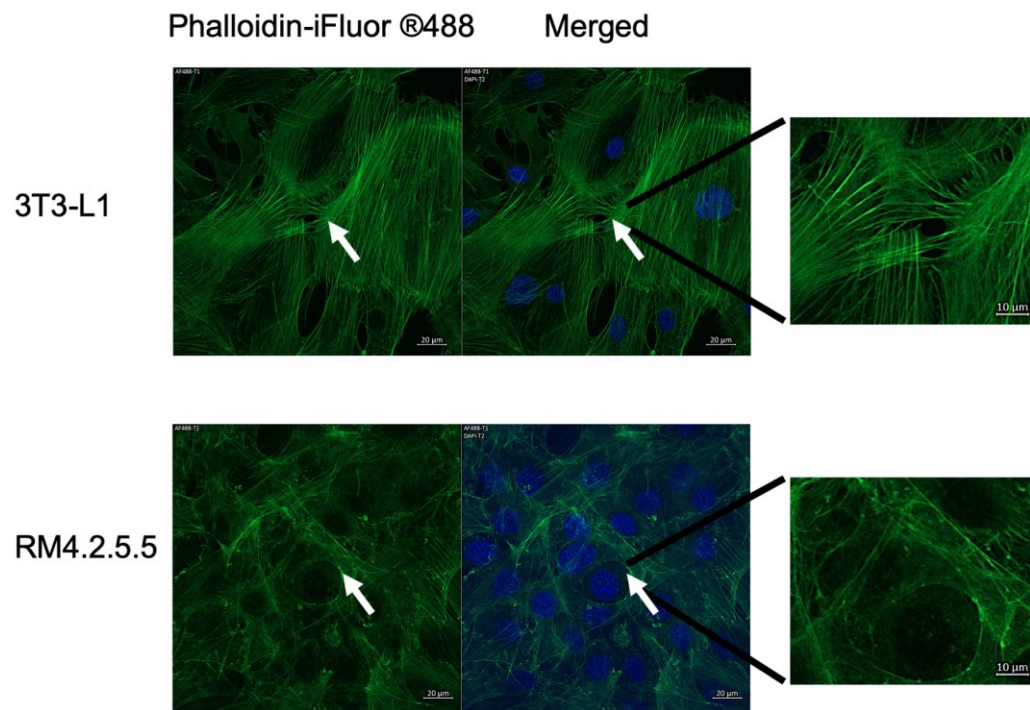
Fig.6



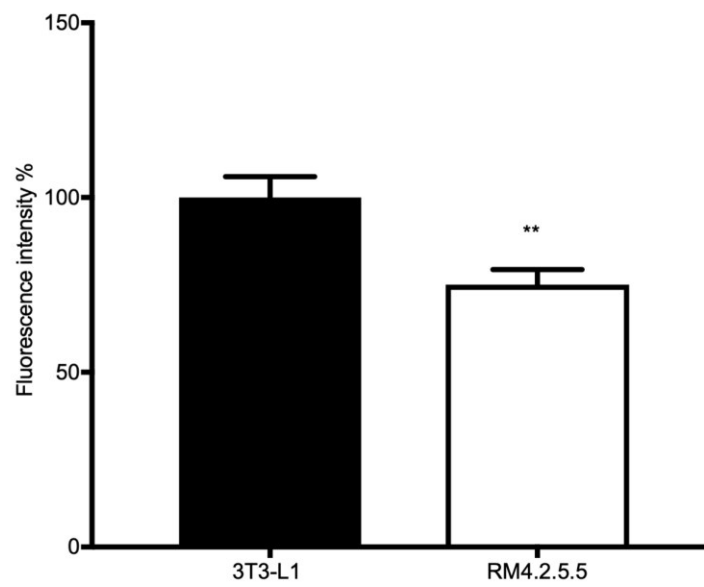
866  
867

Fig.7

A

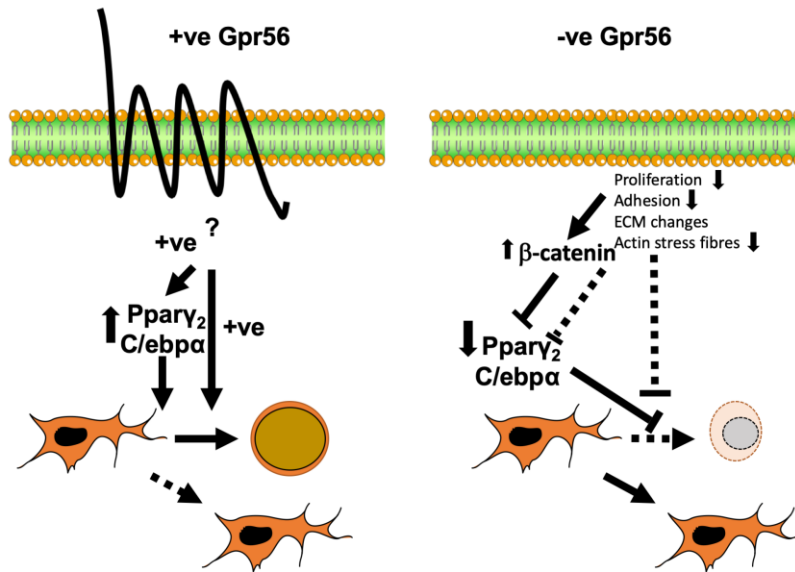


B



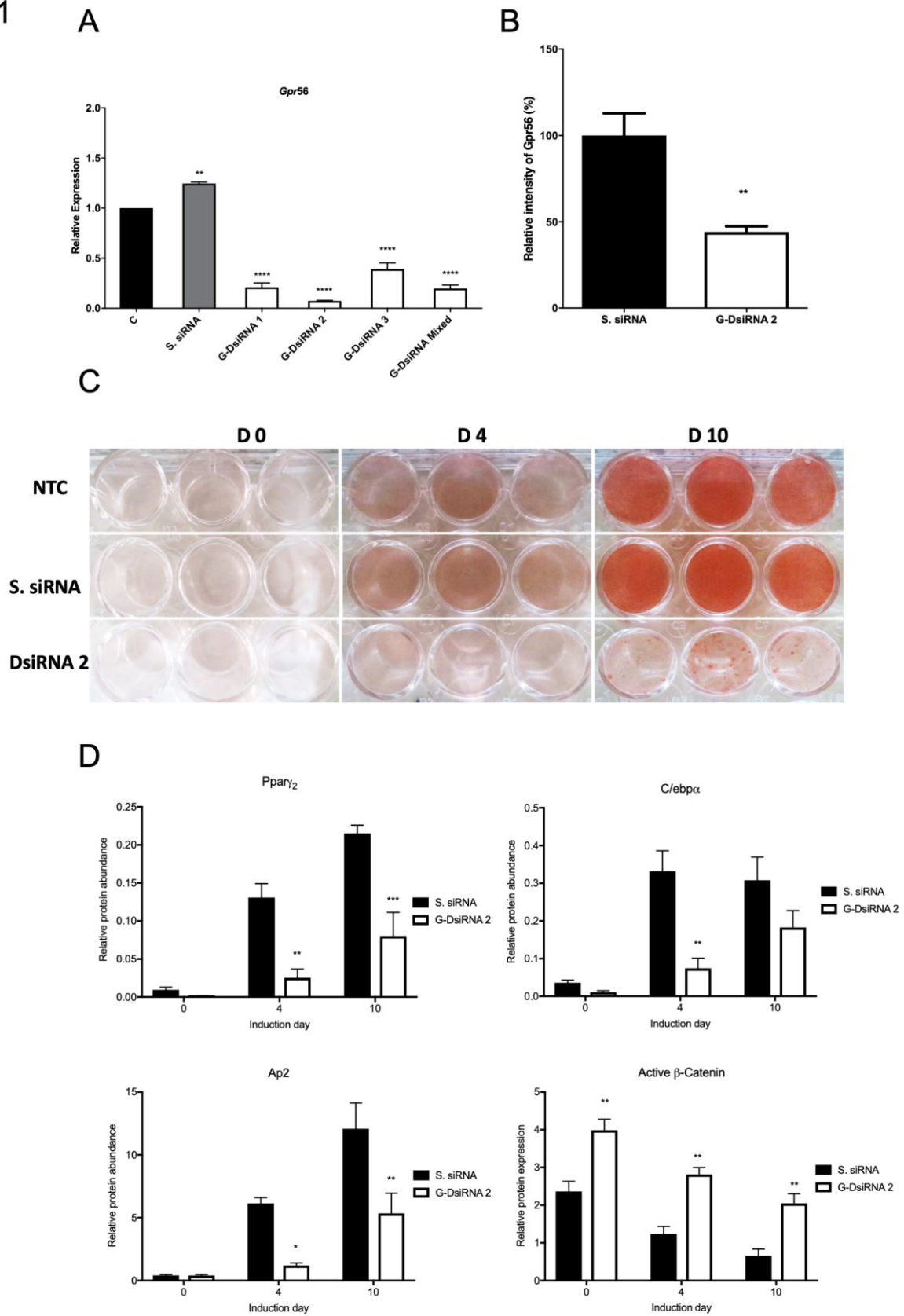
868  
869

Fig.8



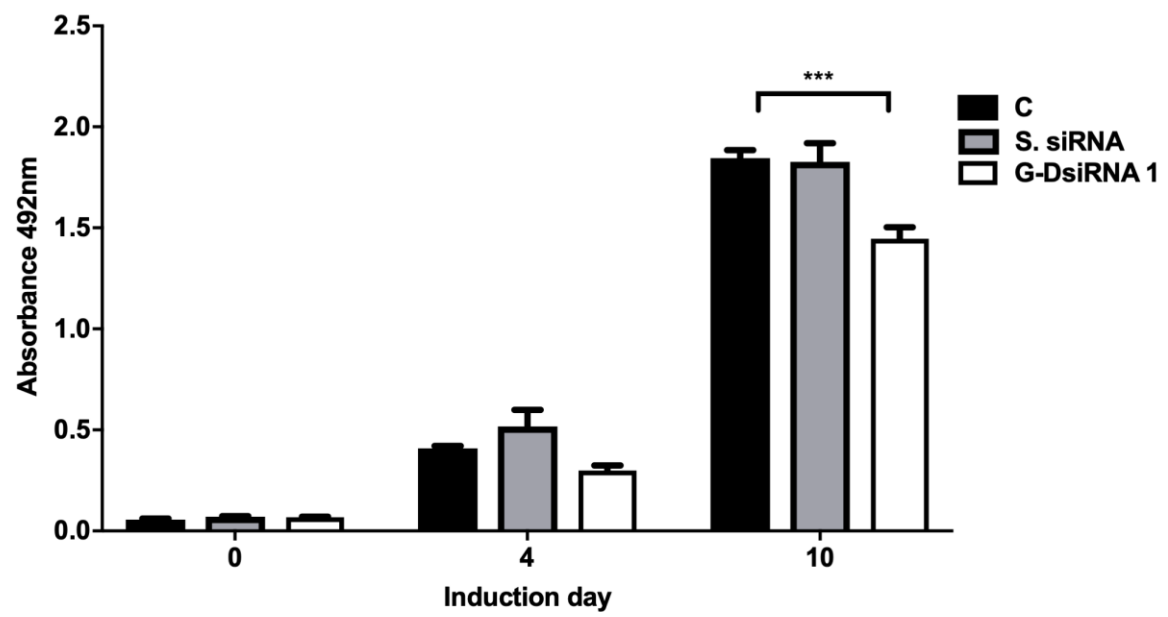
870  
871

S1

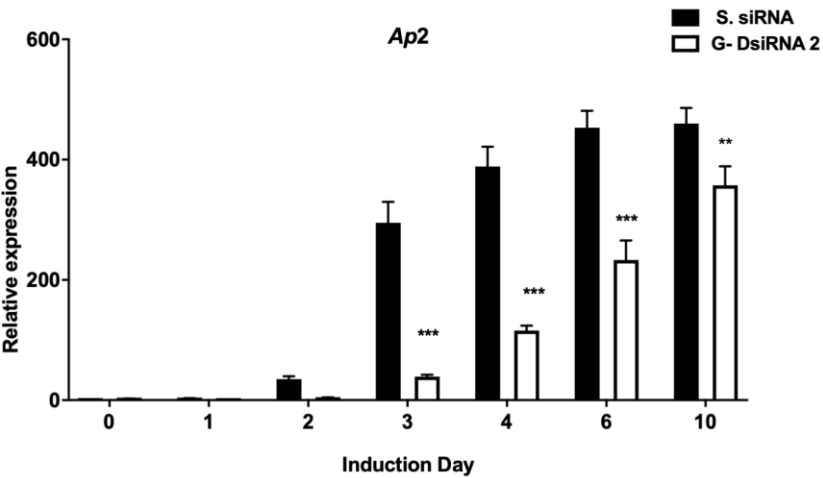
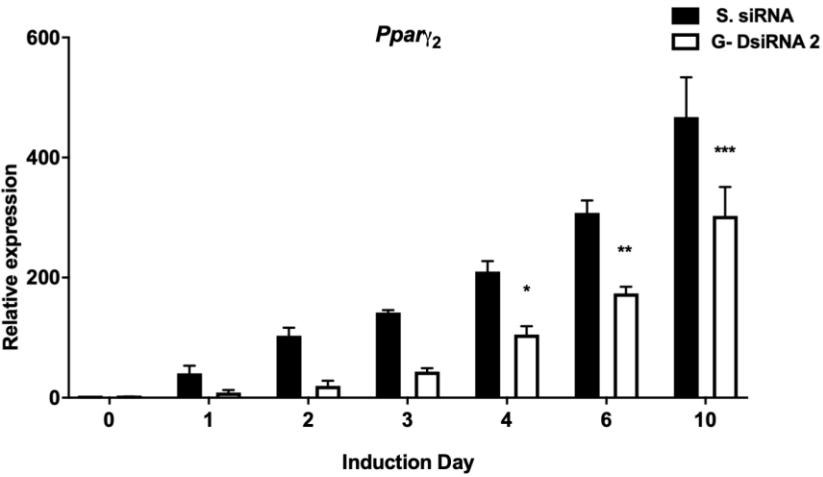


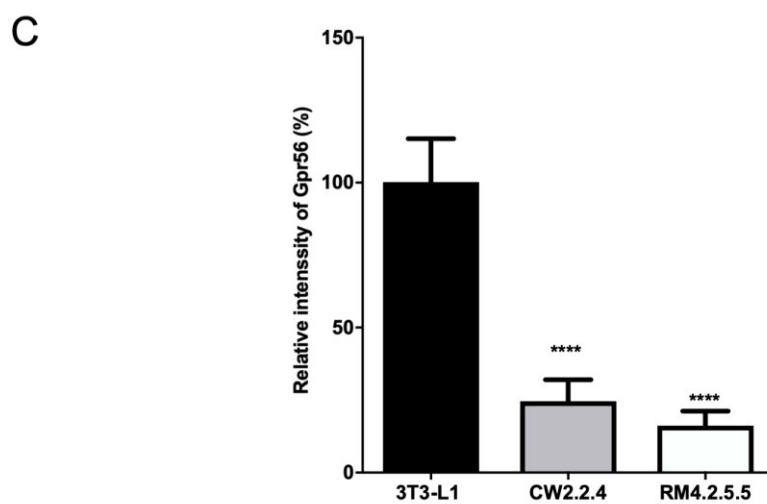
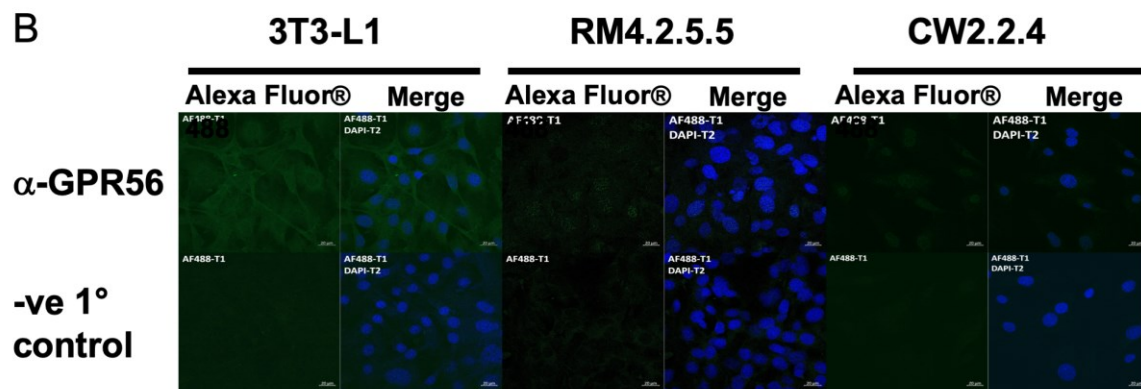
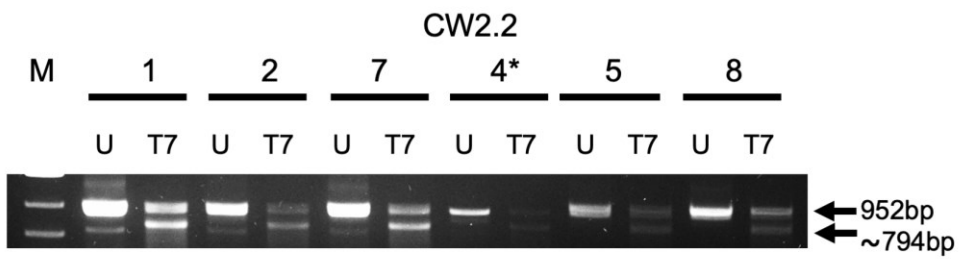
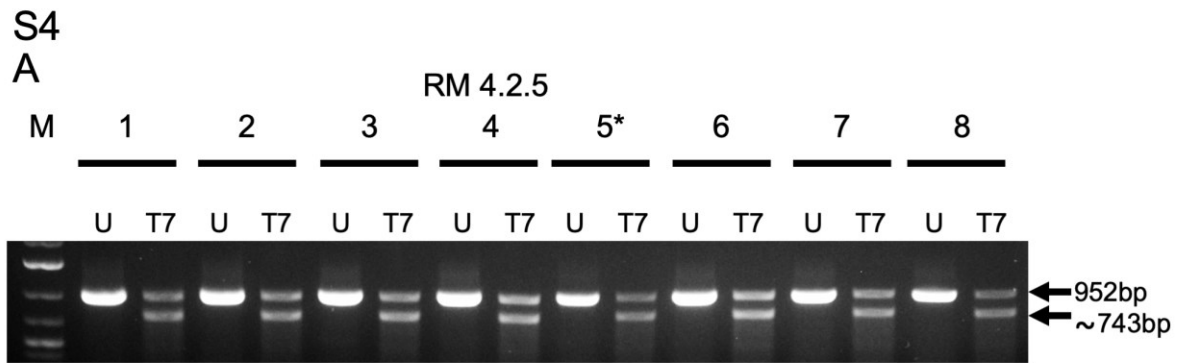
872  
873

S2



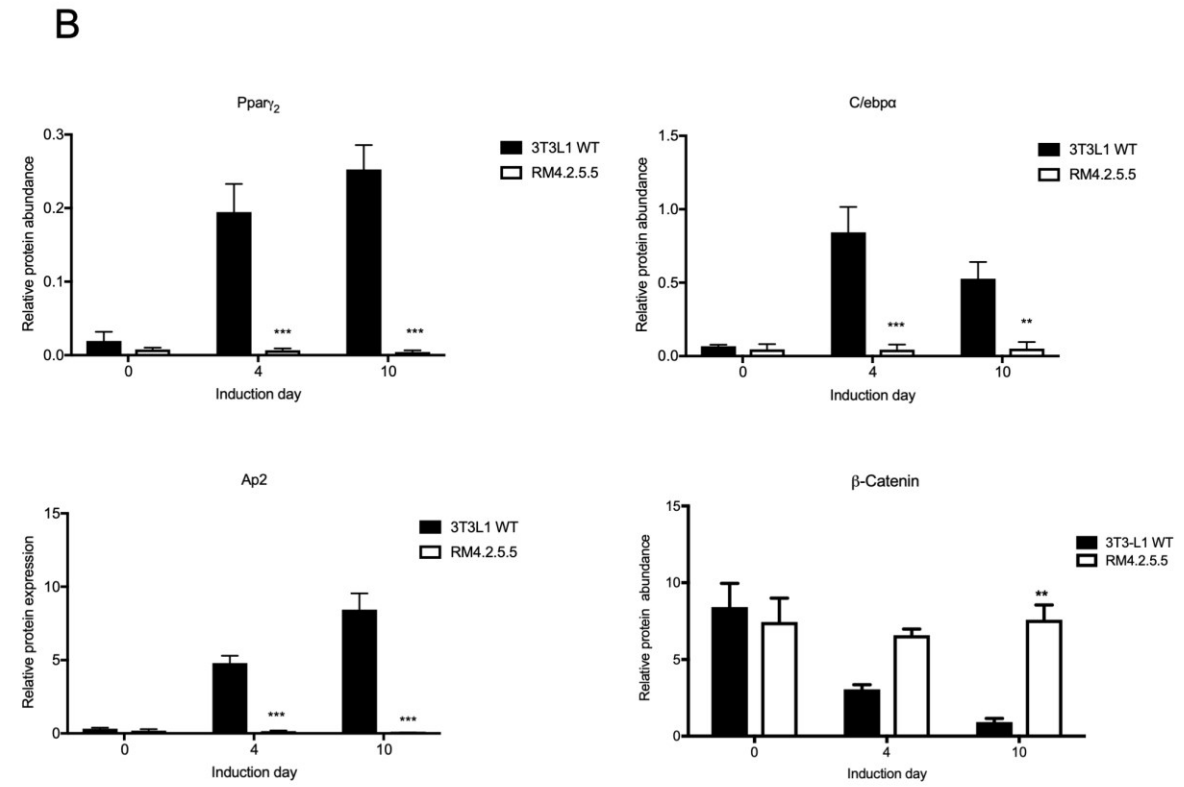
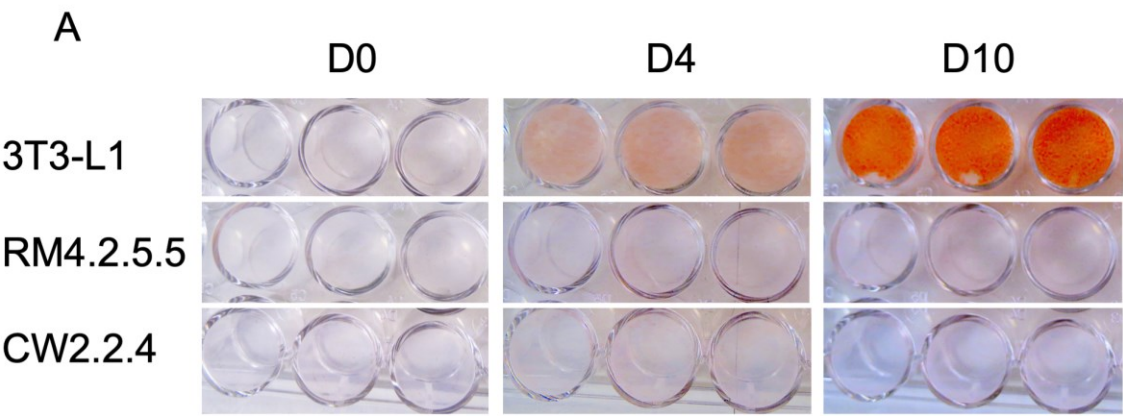
874  
875





878  
879

S5



880  
881



